NAVAL POSTGRADUATE SCHOOL

MONTEREY, CALIFORNIA

THESIS

KNOWLEDGE-BASED ADAPTIVE BEAMSTEERING FOR ENHANCED DETECTION AND INTERFERENCE MITIGATION

by

Monica T. Lavris

December 2021

Thesis Advisor: Ric Romero
Second Reader: Roberto Cristi

THIS PAGE INTENTIONALLY LEFT BLANK

REPORT DOCUMENTATION PAGE			*Form Approved OMB No. 0704-0188*

1. AGENCY USE ONLY *(Leave blank)*	**2. REPORT DATE** December 2021	**3. REPORT TYPE AND DATES COVERED** Master's thesis

4. TITLE AND SUBTITLE KNOWLEDGE-BASED ADAPTIVE BEAMSTEERING FOR ENHANCED DETECTION AND INTERFERENCE MITIGATION	**5. FUNDING NUMBERS**
6. AUTHOR(S) Monica T. Lavris	
7. PERFORMING ORGANIZATION NAME(S) AND ADDRESS(ES) Naval Postgraduate School Monterey, CA 93943-5000	**8. PERFORMING ORGANIZATION REPORT NUMBER**
9. SPONSORING / MONITORING AGENCY NAME(S) AND ADDRESS(ES) N/A	**10. SPONSORING / MONITORING AGENCY REPORT NUMBER**

11. SUPPLEMENTARY NOTES The views expressed in this thesis are those of the author and do not reflect the official policy or position of the Department of Defense or the U.S. Government.

12a. DISTRIBUTION / AVAILABILITY STATEMENT Approved for public release. Distribution is unlimited.	**12b. DISTRIBUTION CODE** A

13. ABSTRACT (maximum 200 words)

Modern-day radar systems continue to increase their adaptability to our changing world. One adaptation is the continued improvement of detection-and-track functionality. Knowledge-based (KB) adaptive beamsteering utilizes a probabilistic representation of a search area to improve overall detection-and-track performance. In this thesis, we consider the search-and-detection problem using adaptive beamsteering for 1-dimensional (1-D) and 2-dimensional (2-D) spatial illumination. We propose a technique that directs the antenna beam on a region of space or cell area with the largest probability as opposed to a popular technique that utilizes the largest uncertainty. To compare detection performance, we allow the whole angular space being interrogated to be interfered with correlated random interference and/or jammers as opposed to discrete interferers. To evaluate performance, we vary the interference or jammer to noise power ratio and the jammer to signal power ratio. The results demonstrate that adaptive beamsteering, when allowed to capitalize on the probability map, can improve detection probability significantly and mitigate random interference and jammer noise.

14. SUBJECT TERMS one-dimensional, two-dimensional, adaptive, antenna, array, beam, beamforming, beamsteering, cognitive, detection, entropy, illumination, interference, jamming, knowledge-based, probabilistic, probability, radar, target, uncertainty	**15. NUMBER OF PAGES** 77
	16. PRICE CODE

17. SECURITY CLASSIFICATION OF REPORT	**18. SECURITY CLASSIFICATION OF THIS PAGE**	**19. SECURITY CLASSIFICATION OF ABSTRACT**	**20. LIMITATION OF ABSTRACT**
Unclassified	Unclassified	Unclassified	UU

NSN 7540-01-280-5500

Standard Form 298 (Rev. 2-89)
Prescribed by ANSI Std. 239-18

THIS PAGE INTENTIONALLY LEFT BLANK

Approved for public release. Distribution is unlimited.

KNOWLEDGE-BASED ADAPTIVE BEAMSTEERING FOR ENHANCED DETECTION AND INTERFERENCE MITIGATION

Monica T. Lavris
Lieutenant, United States Navy
BA, St. Louis University, 2013

Submitted in partial fulfillment of the
requirements for the degree of

MASTER OF SCIENCE IN ELECTRICAL ENGINEERING

from the

NAVAL POSTGRADUATE SCHOOL
December 2021

Approved by: Ric Romero
Advisor

Roberto Cristi
Second Reader

Douglas J. Fouts
Chair, Department of Electrical and Computer Engineering

THIS PAGE INTENTIONALLY LEFT BLANK

ABSTRACT

Modern-day radar systems continue to increase their adaptability to our changing world. One adaptation is the continued improvement of detection-and-track functionality. Knowledge-based (KB) adaptive beamsteering utilizes a probabilistic representation of a search area to improve overall detection-and-track performance. In this thesis, we consider the search-and-detection problem using adaptive beamsteering for 1-dimensional (1-D) and 2-dimensional (2-D) spatial illumination. We propose a technique that directs the antenna beam on a region of space or cell area with the largest probability as opposed to a popular technique that utilizes the largest uncertainty. To compare detection performance, we allow the whole angular space being interrogated to be interfered with correlated random interference and/or jammers as opposed to discrete interferers. To evaluate performance, we vary the interference or jammer to noise power ratio and the jammer to signal power ratio. The results demonstrate that adaptive beamsteering, when allowed to capitalize on the probability map, can improve detection probability significantly and mitigate random interference and jammer noise.

THIS PAGE INTENTIONALLY LEFT BLANK

Table of Contents

List of Figures

List of Acronyms and Abbreviations

1-D	one-dimensional
2-D	two-dimensional
DOD	Department of Defense
JNR	jammer-to-noise ratio
JSR	jammer-to-signal ratio
KB	knowledge-based
KB-MP	knowledge-based maximum probability
KB-ME	knowledge-based maximum entropy
MPDR	minimum power distortionless response
MVDR	minimum variance distortionless response
NPS	Naval Postgraduate School
PAD	power angular density
PSD	power spectral density
Pd	probability of detection
SNR	signal-to-noise ratio
ULA	uniform linear array
UPA	uniform planar array
USN	U.S. Navy

THIS PAGE INTENTIONALLY LEFT BLANK

Acknowledgments

I would like to express my gratitude to my thesis advisor, Dr. Ric Romero, for giving me the opportunity to conduct research and providing me endless devotion and guidance throughout the completion of this work. Without his positive energy, knowledge, and expertise, this thesis would not have been possible.

I would like to also thank Dr. Douglas Fouts, Dr. Roberto Cristi, and LCDR Brannon Chapman for their time and support of this thesis.

Many thanks to the faculty and staff at Naval Postgraduate School for allowing me to continue my education in a field I was unfamiliar with and giving me the opportunity to learn from other great leaders.

THIS PAGE INTENTIONALLY LEFT BLANK

CHAPTER 1:
Introduction

Modern-day radar systems continue to increase their adaptability to our changing world. One adaptation is the continued improvement of detection-and-track functionality. Cognitive radar systems learn about the environment they operate in, provide constant feedback updates, and adjust illumination based on what is learned from the content of radar returns to improve overall performance [1].

Knowledge-based (KB) systems have an interface that allows a decision to be made based off prior knowledge [2]. Cognitive radars use KB adaptive beamsteering, which is a technique to steer a beam to a location to either search and detect a target from the environment or illuminate an already detected target for tracking. Unlike traditional radars where raster scanning may be used to illuminate very large search areas, cognitive radars use a probabilistic approach where it directs the beam at areas of most uncertainty. Per [3], it is often due to the short response time and rapid environmental changes that cognitive radars favor an *a priori* probabilistic approach for better performance.

Extensive use of the tracking functionality is the predominate source of the adaptive capabilities of a cognitive radar, for instance, adaptive beamsteering [3]. In [4], a cognitive radar was developed for a radar system engaged in single target tracking and detection. In [5], a cognitive radar was used for integrated search-and-track applications by the use of channel uncertainty. In [6], a cognitive radar was used for search-and-track application where various uncertainty functions were used to illustrate beamsteering performance and behavior. In this thesis work, we will expand the work in [4], [5], and [6] and consider a radar system that performs adaptive beamsteering for search-and-detection application by capitalizing on the probability map of an area.

1.1 Objective

This thesis presents two objectives in terms of KB adaptive beamsteering. We first propose and compare two adaptive beamsteering design techniques that enhance target detection by utilizing an *a priori* probability map and entropy map approach with the use of both

a uniform linear array (ULA) and a uniform planar array (UPA). Then we evaluate detection performance of adaptive beamsteering to operate in resource-constrained interference environments (e.g., both jamming or friendly sources). These objectives will allow us to accurately steer the antenna main beam in the direction where a target may be present in one or multiple cells in the search area, which is described by the probability or entropy map.

1.2 Scene of Operation

In this thesis, we assume that the radar system has a phased-array antenna (e.g., UPA) and illuminates an environment, where illumination is possible for any type of scenario (e.g., airborne or ground). An example of the radar system illuminating a search area is shown in Figure 1.1. The radar has some *a priori* knowledge of the environment, i.e., the environment has been previously evaluated and the adaptive beamsteering algorithm will conduct a probabilistic approach in steering the beam at the area where target detection is most likely to improve probability of detection.

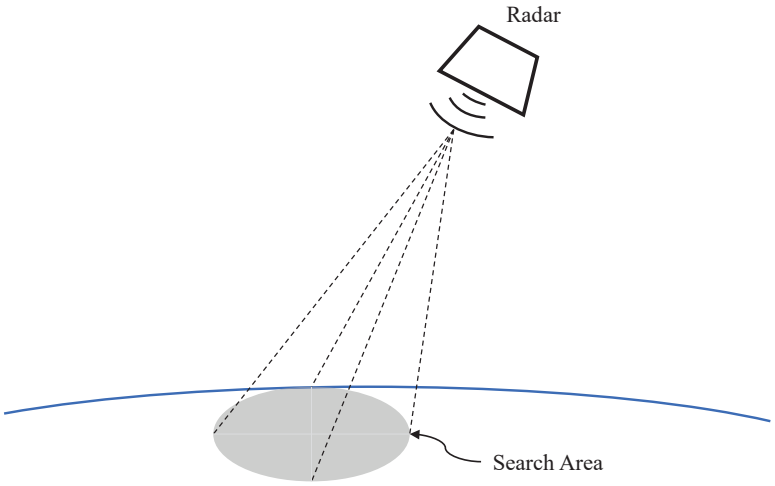

Figure 1.1. Radar scene of operation.

We evaluate multiple scenarios in this thesis from one-dimensional (1-D) to two-dimensional (2-D) search areas where the radar system either illuminates a single cell or multiple cells.

For 1-D illumination, we focus on either azimuth or elevation, whereas in 2-D transmission, we observe in both azimuth and elevation dimensions. For this thesis, we consider the target to be stationary, i.e., no Doppler shift although motion can easily be incorporated [5]. For all scenarios, thermal noise is, of course, present but not always the dominating source as we allow the whole angular space to be interfered with interference/jammers.

1.3 Organization of Thesis

This thesis is organized as follows. In Chapter 2, we describe our signal modeling. In Chapter 3, we present the adaptive beamsteering methodology employed in simulation namely; knowledge-based maximum probability (KB-MP) and knowledge-based maximum entropy (KB-ME) search techniques. In Chapter 4, we evaluate the detection performance of single cell illumination with KB-MP and KB-ME techniques that utilize ULA in noise and interference mitigation. In Chapter 5, we extend our detection performance evaluation and interference mitigation with ULA to a cell area, consisting of multiple cells using the same techniques. In Chapter 6, we evaluate the detection performance of single cell illumination with KB-MP and KB-ME techniques that utilize UPA in noise and interference mitigation. In Chapter 7, we extend our detection performance evaluation and interference mitigation with UPA to a cell area, consisting of multiple cells using the same techniques. Note that single cell illumination indicates a beamwidth corresponds to one cell whereas multiple cell illumination indicates a beamwidth corresponding to a cell area. In Chapter 8, we summarize our conclusions and recommend future work.

THIS PAGE INTENTIONALLY LEFT BLANK

CHAPTER 2:
Signal Modeling

2.1 Spatial Target Model for 1-D

Let the ULA antenna be comprised of N elements where the location of the elements are set by the index vector $\mathbf{n} = [0, 1, ..., N-1]^T$, where T stands for transpose operation. The ULA antenna is shown in Figure 2.1. The probabilistic representation of the search area is a 1-D probability map where *a priori* probabilities of the cells are modeled, known, or calculated from latest observation or measurement.

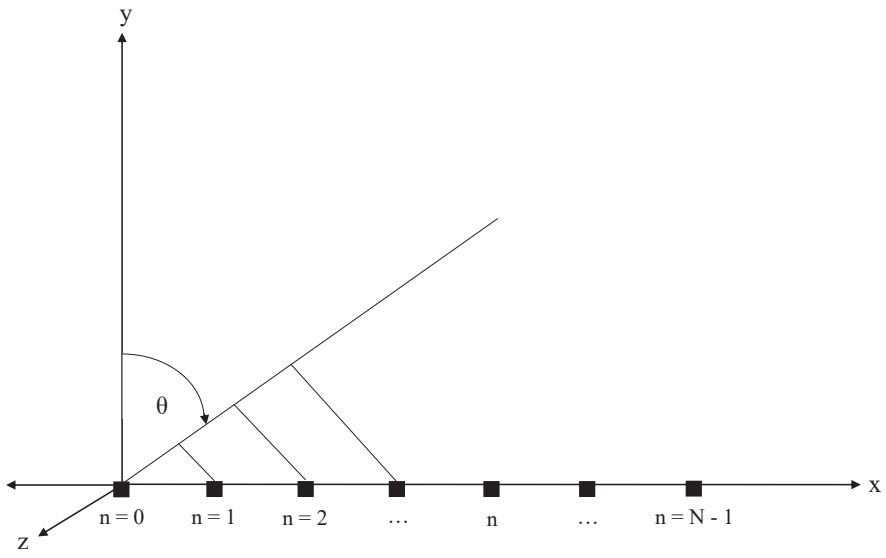

Figure 2.1. Uniform linear array with N elements along the x-axis.

2.2 Spatial Target Model for 2-D

The antenna for the 2-D search scenario is a UPA with $N \times M$ elements. If $N = M$ then we have a case where the UPA is constructed into a matrix of equal rows and columns. For the UPA antenna, shown in Figure 2.2, the location of the element indices are given by the index vectors $\mathbf{n} = [0, 1, ..., N-1]^T$ and $\mathbf{m} = [0, 1, ..., M-1]^T$. We see in Figure 2.2 that the antenna

beam is steered to u_{kx} and u_{ky}, which are locations in the angular search space u_{ax} for the x-direction and u_{ay} for the y-direction [7]. The probabilistic representation of the search area is a 2-D probability map, which much like in the 1-D case, the *a priori* probabilities of the cells are modeled, known, or calculated from latest observation or measurement.

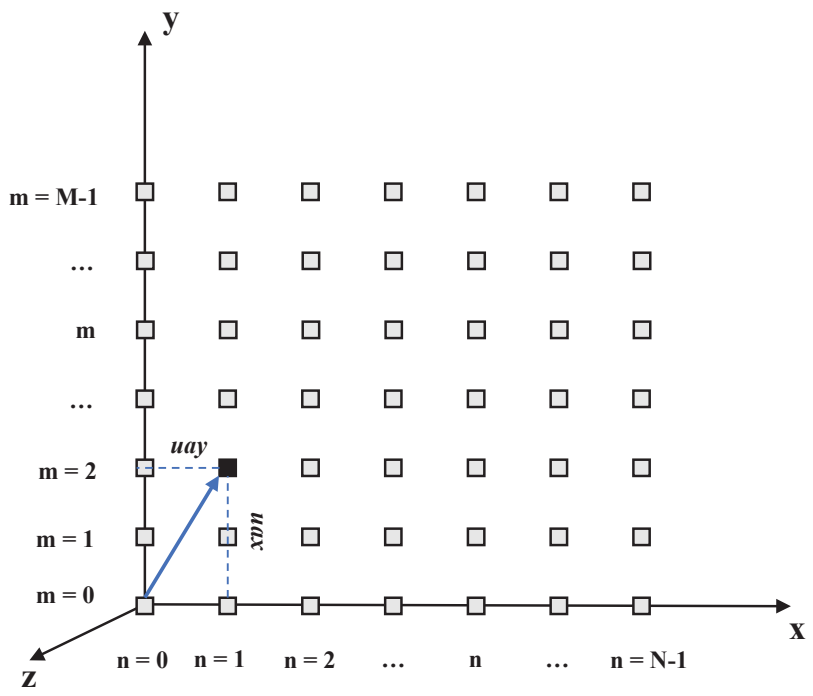

Figure 2.2. Uniform planar array with N elements along the x-axis and M elements along the y-axis; beam is steered to u_{kx} and u_{ky}.

2.3 Knowledge-Based Maximum Probability

As mentioned earlier, prior knowledge of the probability map can be based on the surveillance area being investigated. For example, in a sparse scenario, most probability values are going to be small with very few cells containing high probabilities. The probability values can go from 0 to 1. There are numerous possible models depending on scenarios or previous measurements. In this thesis, we will use a model where a maximum probability exists in the map. For example, a possible maximum is $p_{mx} = 0.9$. Note that the choice is arbitrary and is used purely to evaluate the detection performance of the two KB search approaches.

Thus, for p_{mx} = 0.9, the adaptive beamsteering algorithm, similar to what was used in [6], resorts to illuminating cell areas with larger probabilities than elsewhere. We make the same assumption as in [5] that each cell is independent of another cell. For these simulations, we assume a target can only occupy one cell and 1) a beamwidth corresponds to one cell or 2) a beamwidth corresponds to multiple cells or a cell area.

2.3.1 1-D Array: Single Cell in a Beamwidth

We normalize our angular search area with u_{ax} = {0, $\frac{1}{N}$, ..., 1-$\frac{1}{N}$} where each resolution angle corresponds to a cell. To perform the KB-MP illumination, we select the index of the angle of the plane wave, u_k, that corresponds to the cell in the probability map with the largest probability, which is illustrated in Figure 2.3.

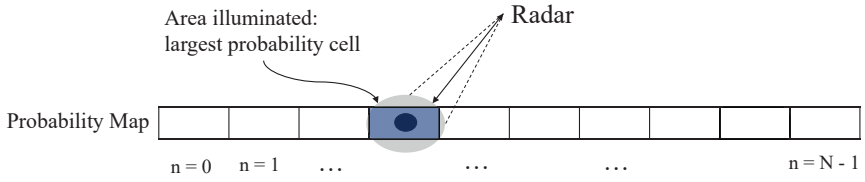

Figure 2.3. 1-D probability map corresponding to the spatial target space. Note that the radar beam illuminates one spatial cell at a time.

The steering vector becomes

$$\mathbf{s}_r = \mathbf{exp}(j2\pi\mathbf{n}u_k), \tag{2.1}$$

where **exp()** is the Euler exponential function and u_k is the normalized angle of the plane wave of interest (here the cell with largest probability).

2.3.2 1-D Array: Multiple Cells in a Beamwidth

The angular search area, u_{ax}, as in Section 2.3.1, is also used for multiple cells inside a beamwidth, where each resolution angle corresponds to a cell area. We transform the probability map to a new probability map, P_{1D}, where the new values are the average probabilities of multiple cells, which is shown in Figure 2.4. The dimensions of P_{1D} reduce from a $N \times 1$ to a $(N-2) \times 1$. For this scenario, we take the average of three cells. Note the

use of three cells in a beamwidth is arbitrary and is used purely to expand the number of cells in a beam and evaluate the detection performance of the two KB search approaches. To perform the KB-MP illumination, we select the index, L, of the angle of the plane wave, u_k, that corresponds to the multiple cells covering a cell area with the largest average probability. Then, the main beam is steered towards that location which is shown in Figure 2.5. The beamwidth covers the index cells of *L-1, L,* and *L+1*.

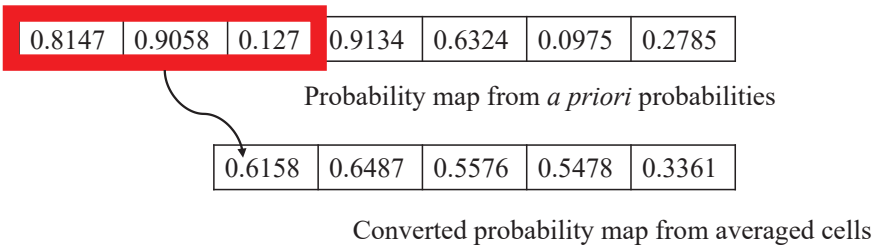

Figure 2.4. Converted 1-D probability map, P_{1D}, from averaged cell probabilities for ULA multiple cells in a beam.

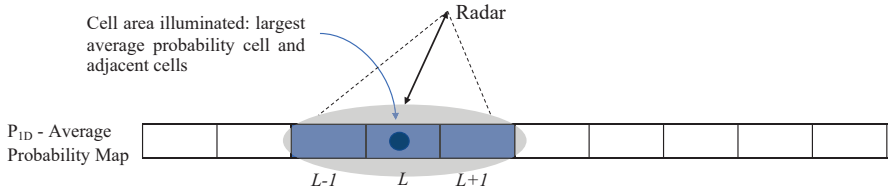

Figure 2.5. 1-D probability map corresponding to spatial target space. Note that the radar beam illuminates multiple spatial cells at a time.

Each cell, corresponding to a different angle of the plane wave, has a steering vector. The steering vectors become

$$\mathbf{v}_{s1} = \mathbf{exp}(j2\pi \mathbf{n} u_{ax}(L\text{-}1)) \tag{2.2}$$

$$\mathbf{v}_{s2} = \mathbf{exp}(j2\pi \mathbf{n} u_{ax}(L)) \tag{2.3}$$

$$\mathbf{v}_{s3} = \mathbf{exp}(j2\pi \mathbf{n} u_{ax}(L\text{+}1)), \tag{2.4}$$

where $u_{ax}()$, as defined above, is the normalized angular search space. In this case, three cells of interest have the largest average probability. The three adjacent angles indexed

by *L-1, L,* and *L+1* correspond to three plane waves of interest. We combine the three steering vectors into one summed steering vector which defines the whole beam. To form a beamformer, which we will discuss in Chapter 3, the effective summed steering vector becomes

$$\mathbf{s}_r = \frac{1}{2}(\mathbf{v_{s1}} + \mathbf{v_{s3}}) + \frac{1}{\sqrt{2}}\mathbf{v_{s2}}, \tag{2.5}$$

where $\mathbf{v_{s1}}$, $\mathbf{v_{s2}}$, and $\mathbf{v_{s3}}$ are the steering vectors for each individual plane angle in the case of multiple cells in a beam. We chose the coefficient values in equation (2.5) to normalize the effective energy to one with the middle steering vector having the larger amplitude. Of course, other weighting techniques are possible.

2.3.3 2-D Array: Single Cell in a Beamwidth

We normalize the angular search area in the x-direction with u_{ax} = {0, $\frac{1}{N}$, ..., 1-$\frac{1}{N}$} and u_{ay} = {0, $\frac{1}{M}$, ..., 1-$\frac{1}{M}$} in the y-direction. Thus, the search area is two-dimensional (azimuth and elevation), where each resolution angle corresponds to a cell. To illuminate the chosen cell, we select the 2-D coordinate index (u_{kx},u_{ky}) corresponding to the largest probability, which is shown in Figure 2.6.

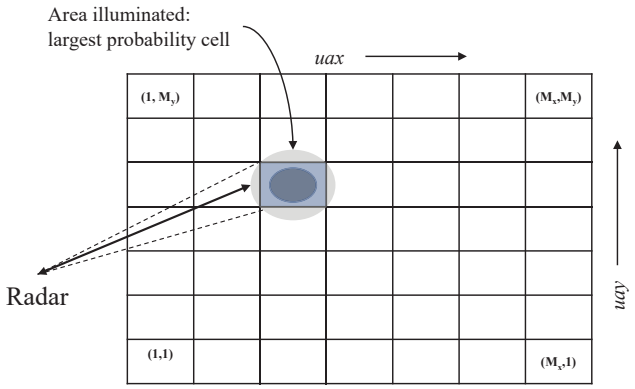

Figure 2.6. 2-D probability map corresponding to spatial target space. Note that the radar beam illuminates one spatial cell at a time.

The steering vector becomes

$$\mathbf{vs}_{uax} = \mathbf{exp}(j2\pi\mathbf{n}u_{kx}) \tag{2.6}$$

for the particular angle in the x-direction and

$$\mathbf{vs}_{uay} = \mathbf{exp}(j2\pi \mathbf{m} u_{ky}) \tag{2.7}$$

for the particular angle in the y-direction. The effective steering vector becomes

$$\mathbf{s}_r = \sqrt{E}\mathbf{vs}_{uax} \otimes \mathbf{vs}_{uay}, \tag{2.8}$$

where $\otimes$ is the Kronecker product, E is energy, and $\mathbf{vs}_{uax}$ and $\mathbf{vs}_{uay}$ are the respective steering vectors for the particular angle in the x and y-directions.

2.3.4 2-D Array: Multiple Cells in a Beamwidth

The normalized angular search area, as described in Section 2.3.3, is utilized. We convert the 2-D probability map into a new 2-D probability map, P_{2D}, where the new probability values are the average probabilities from multiple cells, which is illustrated in Figure 2.7. In this particular case, we consider a cell area of multiple cells made up of four nearby adjacent cells. As such, the dimensions of P_{2D} reduce from a $N \times M$ to a $(N-1) \times (M-1)$.

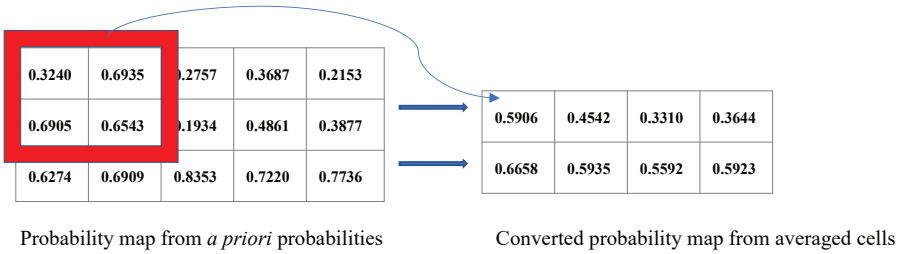

Figure 2.7. Converted 2-D probability map, P_{2D}, from averaged cell probabilities for UPA multiple cells in a beam.

Note the use of four cells is arbitrary and is used purely to expand the number of cells in a beam and evaluate the detection performance of the two KB search approaches. In other words, a beam containing six cells (3×2) or more is easily configured. To illuminate the cell area corresponding to the largest average probability, we select the 2-D coordinate index $L_{x,y}$ in the 2-D plane wave (u_{ax}, u_{ay}) as shown in Figure 2.8. We define the beam to cover four cells by the index found in the matrix below.

$$\begin{bmatrix} L_{x,y} & L_{x+1,y} \\ L_{x,y+1} & L_{x+1,y+1} \end{bmatrix}$$

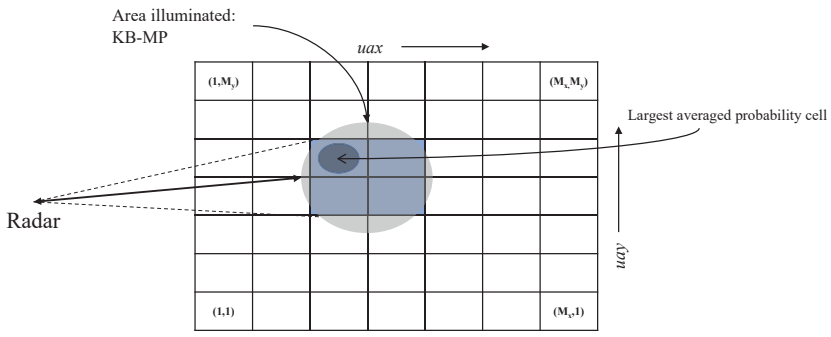

Figure 2.8. 2-D probability map corresponding to spatial target space. Note that the radar beam illuminates multiple spatial cells at a time.

The steering vectors become

$$\mathbf{vs}_{uax} = \mathbf{exp}(j2\pi\mathbf{n}u_{kx}) \tag{2.9}$$

for the particular angles in the x-direction and

$$\mathbf{vs}_{uay} = \mathbf{exp}(j2\pi\mathbf{m}u_{ky}) \tag{2.10}$$

for the particular angles in the y-direction. The effective steering vector becomes

$$\mathbf{s}_r = \sqrt{E}\mathbf{vs}_{uax} \otimes \mathbf{vs}_{uay}, \tag{2.11}$$

where $L_{x,y}$ and $L_{x+1,y}$ are the x-dimension indices used for u_{kx}, $L_{x,y}$ and $L_{x,y+1}$ are the y-dimension indices used for u_{ky}, and $\mathbf{vs}_{uax}$ and $\mathbf{vs}_{uay}$ are the respective steering vectors for the particular angles in the x and y-directions.

2.4 Knowledge-Based Maximum Entropy

Previous probabilistic approaches often aim to select the variable with the most uncertainty [8]. Uncertainty describes an indeterminate that exists within a measurement. Since entropy [9] is a measure of uncertainty, the probability map can be transformed to an uncertainty map, i.e., entropy map. We transform our 1-D probability map vector, $\mathbf{p} = [p_0, p_1, ..., p_{N-1}]^T$, into a 1-D entropy map vector, $\mathbf{h}_e$, and we transform our 2-D probability map matrix,

$$\mathbf{P} = \begin{bmatrix} p_{0,0} & \cdots & p_{0,M-1} \\ \vdots & \ddots & \vdots \\ p_{N-1,0} & \cdots & p_{N-1,M-1} \end{bmatrix}$$

into a 2-D entropy map matrix, $\mathbf{H}_e$. Each entropy vector/matrix element is described by the following equation

$$h = -p\log_2(p) - (1-p)\log_2(1-p), \tag{2.12}$$

where $\log_2$ is base 2 logarithm.

Like cell probabilities, the cell entropies are always positive. Following the scenario-specific probability modeling in the previous sections, our entropy can have a maximum uncertainty of $u_{mx} = 1$. Using the assumptions in [5], the adaptive beamsteering algorithm "will seek to minimize total system uncertainty by pointing the beam at the region of search space with the greatest uncertainty" [6].

2.4.1 1-D Array: Single Cell in a Beamwidth

To illuminate the cell with the largest uncertainty in a 1-D search area where a single cell corresponds to a beamwidth, we select the index of the angle of the plane wave, u_{ke}, corresponding to the vector element in $\mathbf{h}_e$ with the largest entropy, which is shown in Figure 2.9. The steering vector becomes

$$\mathbf{s}_{re} = \mathbf{exp}(j2\pi\mathbf{n}u_{ke}), \tag{2.13}$$

where u_{ke} is the normalized angle of the plane wave of interest corresponding to the cell with the largest entropy.

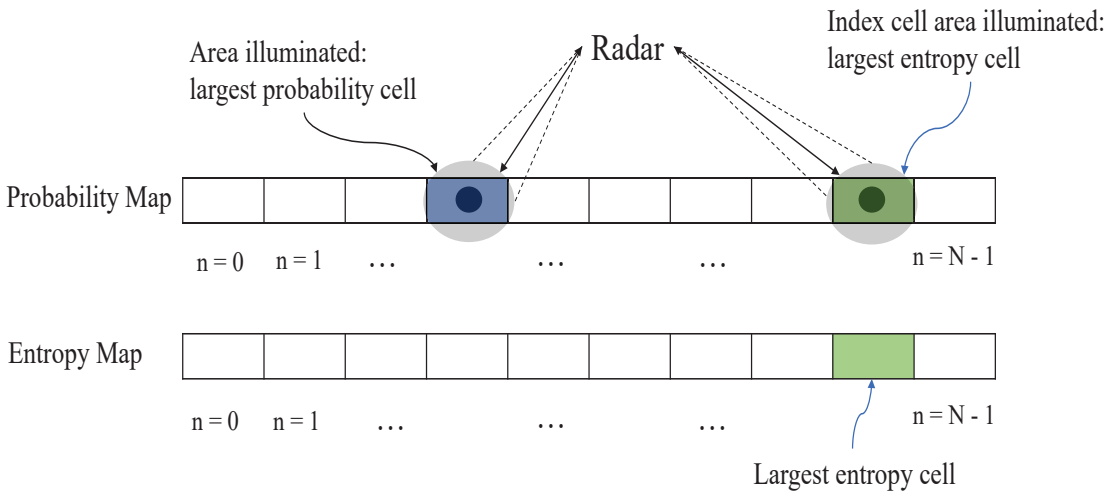

Figure 2.9. Cell illumination with the use of probability and entropy maps of the spatial target space. Note that the radar beam illuminates one spatial cell at a time.

2.4.2 1-D Array: Multiple Cells in a Beamwidth

To illuminate the cell area with the largest average uncertainty, we select the index, L, of the angle of the plane wave, u_{ke}, that corresponds to the multiple cells covering a cell area in the vector element in $\mathbf{h}_e$ with the largest average entropy as shown in Figure 2.10. The beamwidth covers the index cell areas of *L-1, L*, and *L+1* corresponding to the plane waves that yield the largest average entropy. Each cell area, corresponding to a different angle of the plane wave, has a steering vector. The steering vectors become

$$\mathbf{vse}_1 = \mathbf{exp}(j2\pi\mathbf{n}u_{ke}(L\text{-}1)) \tag{2.14}$$

$$\mathbf{vse}_2 = \mathbf{exp}(j2\pi\mathbf{n}u_{ke}(L)) \tag{2.15}$$

$$\mathbf{vse}_3 = \mathbf{exp}(j2\pi\mathbf{n}u_{ke}(L\text{+}1)), \tag{2.16}$$

where u_{ke}, as defined above, is the normalized angular search space. Again, three cells of interest have the largest average entropy. We combine the three steering vectors into one summed steering vector which defines the whole beam. To form a beamformer, which we

will discuss in Chapter 3, the effective summed steering vector becomes

$$\mathbf{s}_{re} = \frac{1}{2}(\mathbf{vse}_1 + \mathbf{vse}_3) + \frac{1}{\sqrt{2}}\mathbf{vse}_2, \tag{2.17}$$

where the coefficient values in equation (2.17) are chosen to normalize the effective energy to one with the middle steering vector, again, having the larger amplitude. Of course, other weighting techniques are possible.

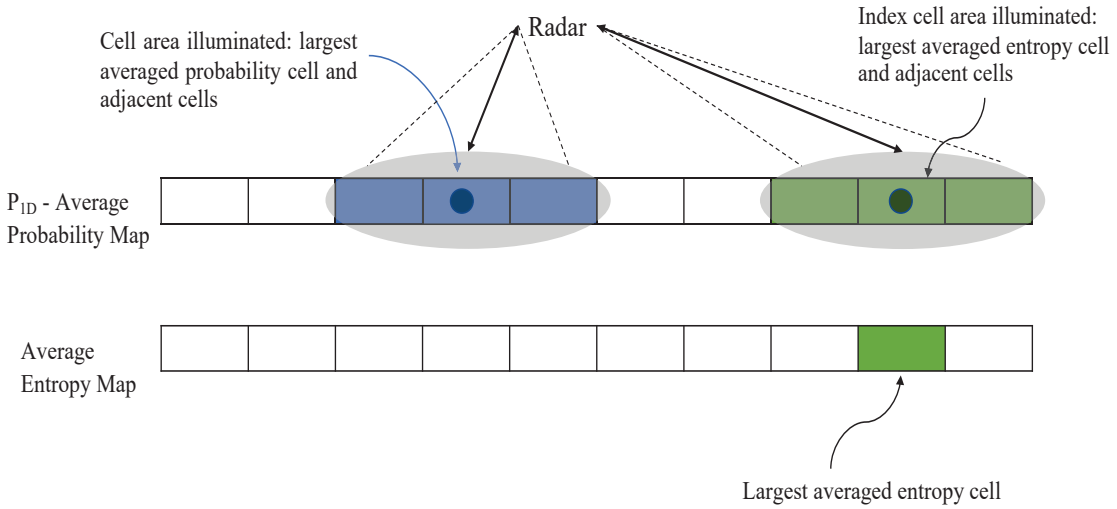

Figure 2.10. Cell illumination with the use of probability and entropy maps of the spatial target space. Note that the radar beam illuminates multiple spatial cells at a time.

2.4.3 2-D Array: Single Cell in a Beamwidth

Recall that the search area is two-dimensional (azimuth and elevation), where each resolution angle corresponds to a cell. To illuminate the cell with the largest uncertainty, we select the 2-D coordinate index (u_{kex}, u_{key}) that corresponds the largest entropy in the matrix element, $\mathbf{H}_e$, which is shown in Figure 2.11. The steering vector becomes

$$\mathbf{vse}_{uax} = \mathbf{exp}(j2\pi\mathbf{n}u_{kex}) \tag{2.18}$$

for the particular angle in the x-direction and

$$\mathbf{vse}_{uay} = \mathbf{exp}(j2\pi \mathbf{m} u_{key}) \tag{2.19}$$

for the particular angle in the y-direction. The effective steering vector becomes

$$\mathbf{s}_{re} = \sqrt{E}\mathbf{vse}_{uax} \otimes \mathbf{vse}_{uay}, \tag{2.20}$$

where $\mathbf{vse}_{uax}$ and $\mathbf{vse}_{uay}$ are the respective steering vectors for the particular angle in the x and y-directions.

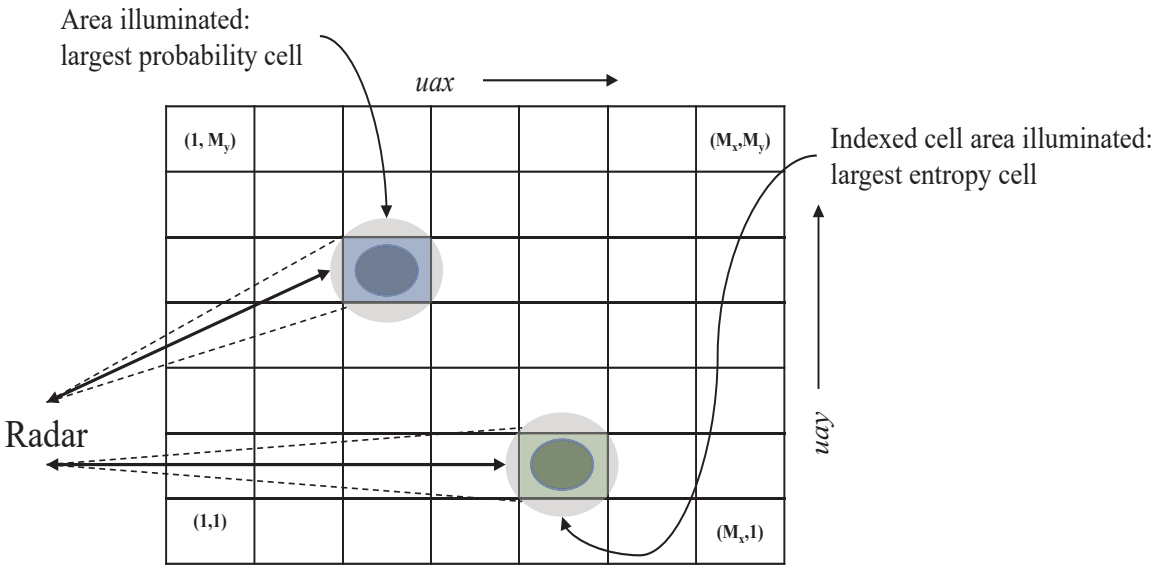

Figure 2.11. Cell illumination with the use of 2-D probability and entropy maps of the spatial target space. Note that the radar beam illuminates one spatial cell at a time.

2.4.4 2-D Array: Multiple Cells in a Beamwidth

To illuminate the cell area with the largest average uncertainty, we select the 2-D coordinate index $L_{xe,ye}$ in the 2-D plane wave (u_{ax}, u_{ay}) which is shown in Figure 2.12. As in Section 2.3.4, we consider a cell area of multiple cells made up of four nearby adjacent cells which

can be found in the matrix below.

$$\begin{bmatrix} L_{xe,ye} & L_{xe+1,ye} \\ L_{xe,ye+1} & L_{xe+1,ye+1} \end{bmatrix}$$

The steering vectors become

$$\mathbf{vse}_{uax} = \mathbf{exp}(j2\pi\mathbf{n}u_{kex}) \tag{2.21}$$

for the particular angles in the x-direction and

$$\mathbf{vse}_{uay} = \mathbf{exp}(j2\pi\mathbf{m}u_{key}) \tag{2.22}$$

for the particular angles in the y-direction. The effective steering vector becomes

$$\mathbf{s}_{re} = \sqrt{E}\mathbf{vse}_{uax} \otimes \mathbf{vse}_{uay}, \tag{2.23}$$

where $L_{xe,ye}$ and $L_{xe+1,ye}$ are the x-dimension indices used for u_{kex}, $L_{xe,ye}$ and $L_{xe,ye+1}$ are the y-dimension indices used for u_{key}, and $\mathbf{vse}_{uax}$ and $\mathbf{vse}_{uay}$ are the respective steering vectors for the particular angles in the x and y-directions.

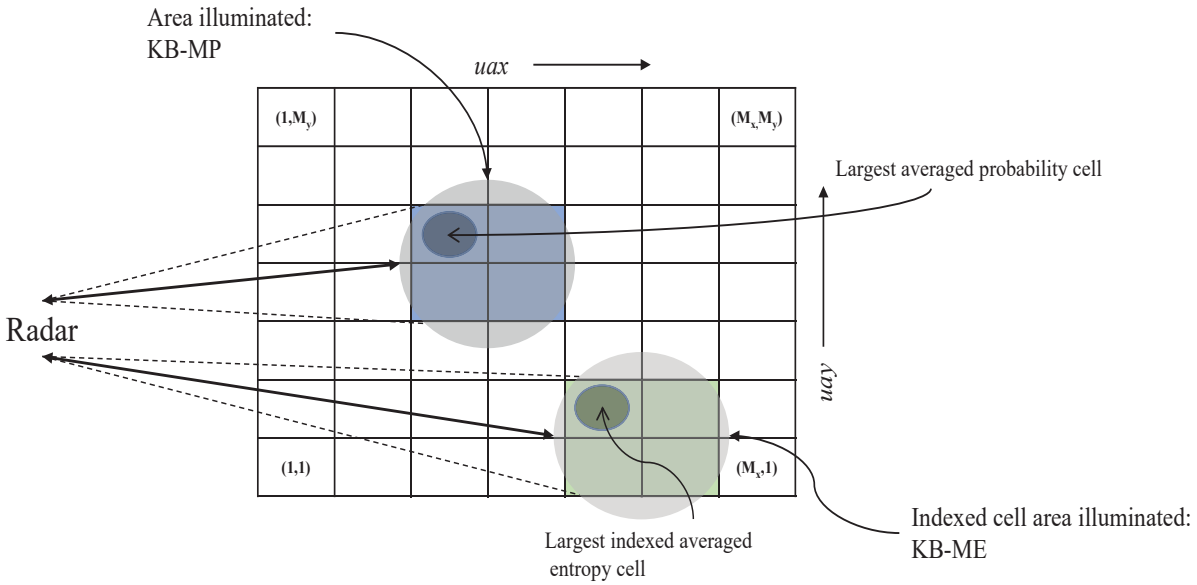

Figure 2.12. Cell illumination with the use of 2-D probability and entropy maps of the spatial target space. Note that the radar beam illuminates multiple spatial cells at a time.

THIS PAGE INTENTIONALLY LEFT BLANK

CHAPTER 3:
Adaptive Beamsteering for Search and Detection

3.1 Beamsteering Selection and Detection Problem

Recall our adaptive beamsteering algorithm considers two approaches for directing the beam on a region of space: 1) KB-MP, which illuminates the cell or cell area with largest probability and 2) KB-ME, which illuminates the cell or cell area with largest uncertainty (entropy). We will investigate four separate experiments utilizing both approaches to evaluate target detection performance in receiver-only (thermal) noise and in resource-constrained interference environments for 1-D and 2-D cases.

Considering the target present hypothesis in our detection problem, the received signal, $\mathbf{x}$, is given by

$$\mathbf{x} = \mathbf{s}_r + \mathbf{n} + \mathbf{s}_{in} \tag{3.1}$$

for KB-MP and

$$\mathbf{x} = \mathbf{s}_{re} + \mathbf{n} + \mathbf{s}_{in} \tag{3.2}$$

for KB-ME, where $\mathbf{s}_r$ and $\mathbf{s}_{re}$ are the signals to be detected, $\mathbf{n}$ is thermal noise, and $\mathbf{s}_{in}$ is interference. For the null hypothesis (i.e. the target is not present in the cell being interrogated), then $\mathbf{s}_r$ and $\mathbf{s}_{re}$ are removed from equations (3.1) and (3.2).

3.2 Optimum Beamformer

From maximizing the output signal-to-noise ratio (SNR) to minimizing the power distortionless response (MPDR), beamformers optimize the metrics they are designed for to either detect or estimate the desired signal [7]. In this thesis, we employ the beamformer called minimum variance distortionless response (MVDR) technique. We consider the signal to be detected, $\mathbf{s}_r$ or $\mathbf{s}_{re}$, as defined in Chapter 2 for the various scenarios. For the KB-MP technique, the MVDR beamformer is described by the following equations:

$$\lambda_{\mathbf{s}} = [\mathbf{s}_r^H \mathbf{S}_n^{-1} \mathbf{s}_r]^{-1} \tag{3.3}$$

and

$$\mathbf{w}_{mvdr}^{H} = \lambda_s \mathbf{s}_r^H \mathbf{S}_n^{-1}. \tag{3.4}$$

For KB-ME technique, the beamformer is described by the following equations:

$$\lambda_{\mathbf{s}} = [\mathbf{s}_{re}^H \mathbf{S}_n^{-1} \mathbf{s}_{re}]^{-1} \tag{3.5}$$

and

$$\mathbf{w}_{mvdr}^{H} = \lambda_s \mathbf{s}_{re}^H \mathbf{S}_n^{-1}, \tag{3.6}$$

where λ_s is the Lagrange multiplier, $\mathbf{S}_n$ is the covariance matrix of the noise and interference, and $\mathbf{w}_{mvdr}^{H}$ is the optimum MVDR weights for the desired signal plus noise, where H is the Hermitian operator [7].

3.3 Random Interference/Jammers

The solution in which a discrete jammer or friendly interferer is known to be at a certain angle is a well known problem in which the obvious solution is via nulling [7]. Our interest is when all of the angles may contain interference and such interference power is modeled probabilistically where each angle's interference may be considered independent or correlated to another. The power angular density (PAD, which is the spatial equivalent to random process's power spectral density (PSD)) that describes the interference in our simulations is a Hamming window with complex-valued realizations. In other words, jammers/interferers may inhabit the entire search area and have random amplitudes. Indeed, we actually allow jammers to be in the same angle/cell as the radar return as opposed to common problems where the jammer and target signal occupy separate angular plane waves and thus, the jammer is easily mitigated. The Hamming window used for simulation in the 1-D models is shown in Figure 3.1, where the x-axis is defined by normalized search space which we defined as a set of angles u_{ax} but can also be thought of as the angular vector, $\mathbf{u}_{ax}$ just like the index vector $\mathbf{n}$. In other words, if the target or angle of the plane wave is directed in the main lobe of the Hamming window, our beam is steered into more interference.

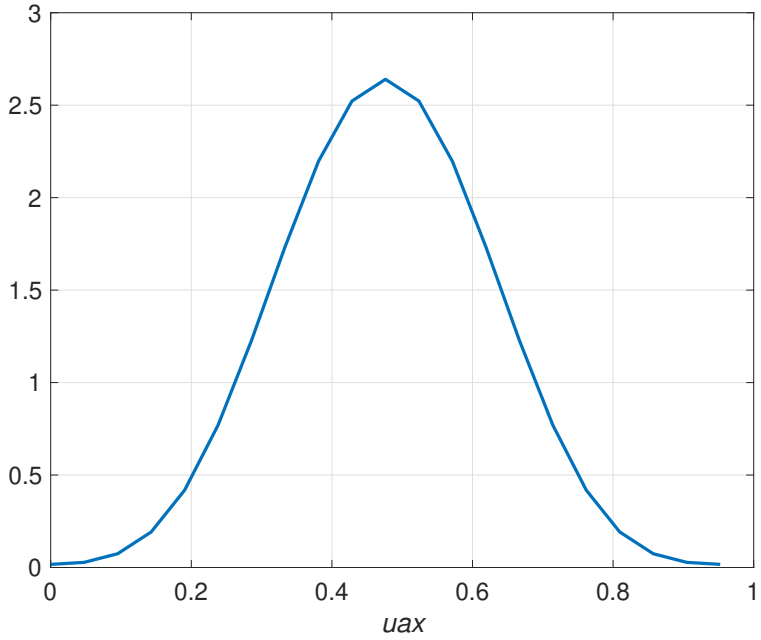

Figure 3.1. 1-D Hamming window interference model.

In the case of 2-D search space where a 2-D interference model is needed, we use the same Hamming window for $\mathbf{u}_{ay}$ (which is repeated for all values of $\mathbf{u}_{ax}$). Other models are easily incorporated such as a 2-D Hamming interference model. The intensity map corresponding to the PAD of the current 2-D interference is shown in Figure 3.2, where the x-axis and y-axis are defined by normalized search space with angular vectors, $\mathbf{u}_{ax}$ and $\mathbf{u}_{ay}$. In other words, every $\mathbf{u}_{ax}$ angular angle (which spans the whole $\mathbf{u}_{ay}$ space) has its own individual PAD described by Hamming window. If the target or angle of the plane wave for both the x and y-directions happens to be in the center of the Hamming window, unfortunately, the beam will be steered into more interference also. This is the consequence of allowing the practical case where interference may be in the same angular space as the plane wave coming from the target. This explains some of the more subtle features of simulation results (which will be discussed later) when this possibility is realized.

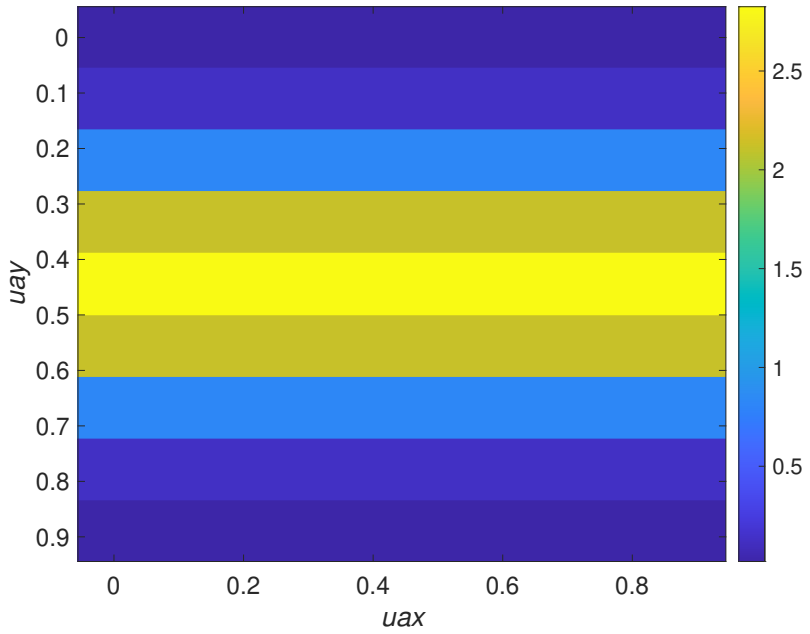

Figure 3.2. 2-D Hamming window interference model (intensity map).

CHAPTER 4:
Uniform Linear Array - Single Cell Performance

4.1 Noise Only

We consider a signal comprised of the target return and thermal noise such that SNR is varied from 0 to 20 dB with 1 dB increments and desired $P_{fa} = 0.001$. In terms of scenario-specific probability models that describe the search area, we assume a model with randomly generated cell probabilities from 0 to maximum probability, p_{mx}, which of course has a corresponding maximum entropy. We then compare the performance of KB-MP and KB-ME techniques while parameterizing p_{mx}, where $p_{mx} = 1$, 0.9, and 0.5. Since the values in the probability map are randomly generated, p_{mx} is not the guaranteed maximum realization in the simulation. Let the variable, p_s, be *a priori* probability of a cell, i.e., the probability realization in a simulation. We conduct a Monte Carlo simulation with 10,000 trials to quantify the probability of detection of a target present in that cell as a function of SNR. There is a subtle yet significant difference from a simple detection problem that we consider in this work. Recall that while *a priori* knowledge informs us of cell probability, it does not guarantee the presence of a target unlike the conditional target present hypothesis in the common detection problem. Thus, in the Monte Carlo simulation, we introduce an indicator variable, p_i, that takes on the value of 1 (target present) and 0 (target not present). For example, if p_s is used, then the ratio of 1's to the number of Monte Carlo trials converges to p_s as the number of trials get large. Then, the received signal in the simulation takes on the equation

$$\mathbf{x} = p_{i,p}\mathbf{s}_r + \mathbf{n} \tag{4.1}$$

for KB-MP and

$$\mathbf{x} = p_{i,e}\mathbf{s}_{re} + \mathbf{n} \tag{4.2}$$

for KB-ME, where $p_{i,p}$ and $p_{i,e}$ are the indicator variables corresponding to the two techniques. The comparison of the probability of detection of a radar using KB-MP and a radar using KB-ME for the cell chosen by each technique is shown in Figure 4.1. In several previous cognitive radar works, maximum uncertainty (via entropy) was utilized but it is

clear that KB-MP has higher probability of detection than KB-ME for p_{mx} of 1 and 0.9. When p_{mx} is 0.5, both KB-MP and KB-ME have similar detection thus, beamsteering to either cell would result in the same detection performance.

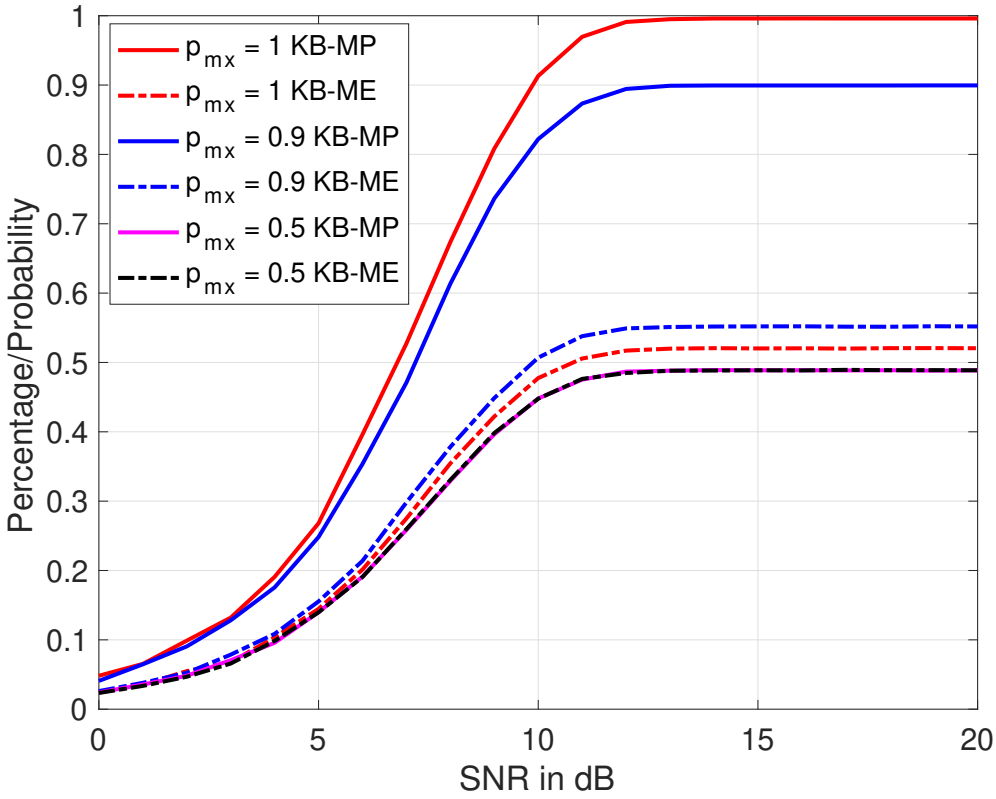

Figure 4.1. P_d results for Experiment 1: interference is thermal noise only, where p_{mx} represents the possible maximum target probability in the *a priori* model in the KB problem formulation.

4.2 Interference or Jamming

We consider a signal comprised of a steering vector, thermal noise, and interference. The received signal in the simulation takes on the equation

$$\mathbf{x} = p_{i,p}\mathbf{s}_r + \mathbf{n} + \mathbf{s}_{in} \tag{4.3}$$

for KB-MP and

$$\mathbf{x} = p_{i,e}\mathbf{s}_{re} + \mathbf{n} + \mathbf{s}_{in} \tag{4.4}$$

for KB-ME. With p_{mx} = 1, 0.9, and 0.5, we see in Figure 4.2 that allowing interference (jammers) to appear in all the angles including the angle with the target return significantly affects detection performance of both KB-MP and KB-ME. When p_{mx} = 0.5, both KB-MP and KB-ME have similar detection. It is clear that if interference is allowed to be in the same angular space as the radar return, detection performance is decreased.

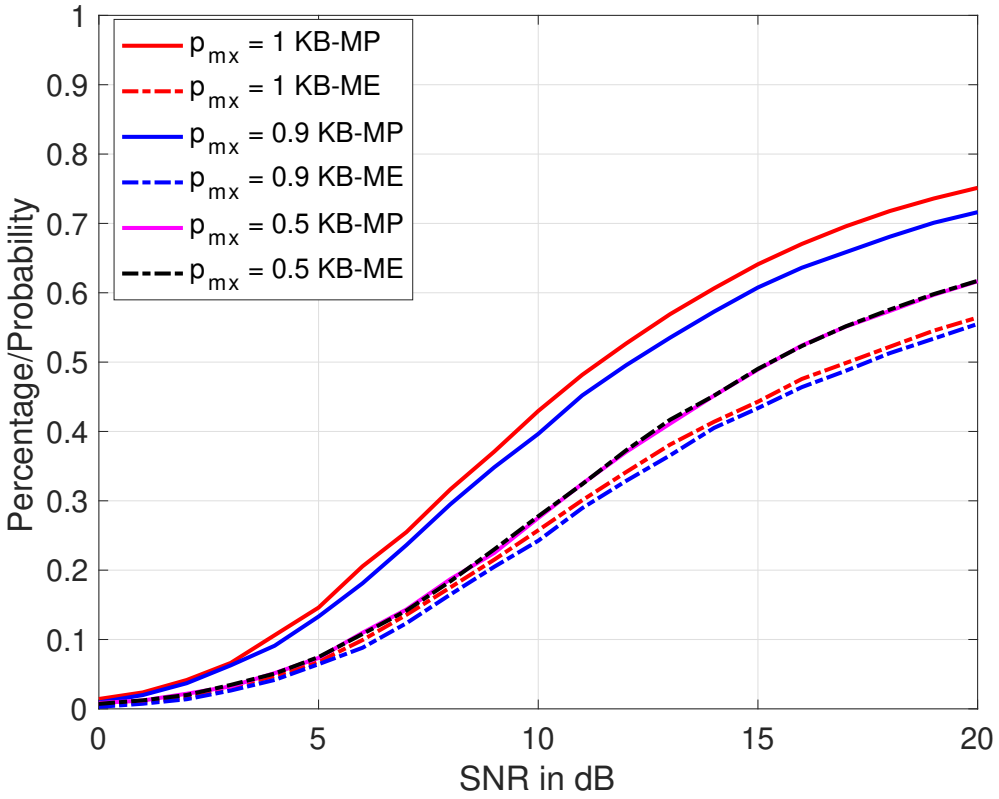

Figure 4.2. P_d results of Experiment 2: total interference consists of random jammer/interference and noise, where p_{mx} represents the possible maximum target probability in the *a priori* model in the KB problem formulation.

4.2.1 Varying JSR

As in Experiment 2, p_{mx} = 0.9 and jammer-to-signal ratio (JSR) is varied at -13 dB, -10 dB, and 0 dB. We see in Figure 4.3 that interference significantly affects detection performance of both KB-MP and KB-ME. Increasing the jammer power significantly lowers the detection performance. The Hamming window utilized for interference is illustrated in Figure 4.4, where it is clear the cell chosen by KB-MP technique contains more interference than the cell chosen by KB-ME technique. Due to this, we see in Figure 4.3, that as SNR and JSR are increased, a crossover in performance occurs. Typically, as observed already, KB-MP has better detection than KB-ME. This is mostly true in the case of JSR = -10 and -13 dB. Note however, that at very large SNR, P_d for KB-ME is better than KB-MP. This is because the angle chosen by the entropy method has less interference as shown in Figure 4.4. In other words, P_d is affected by both *a priori* cell probabilities and interference power. Ultimately, the performance of KB-MP and KB-ME depends on the value of both parameters.

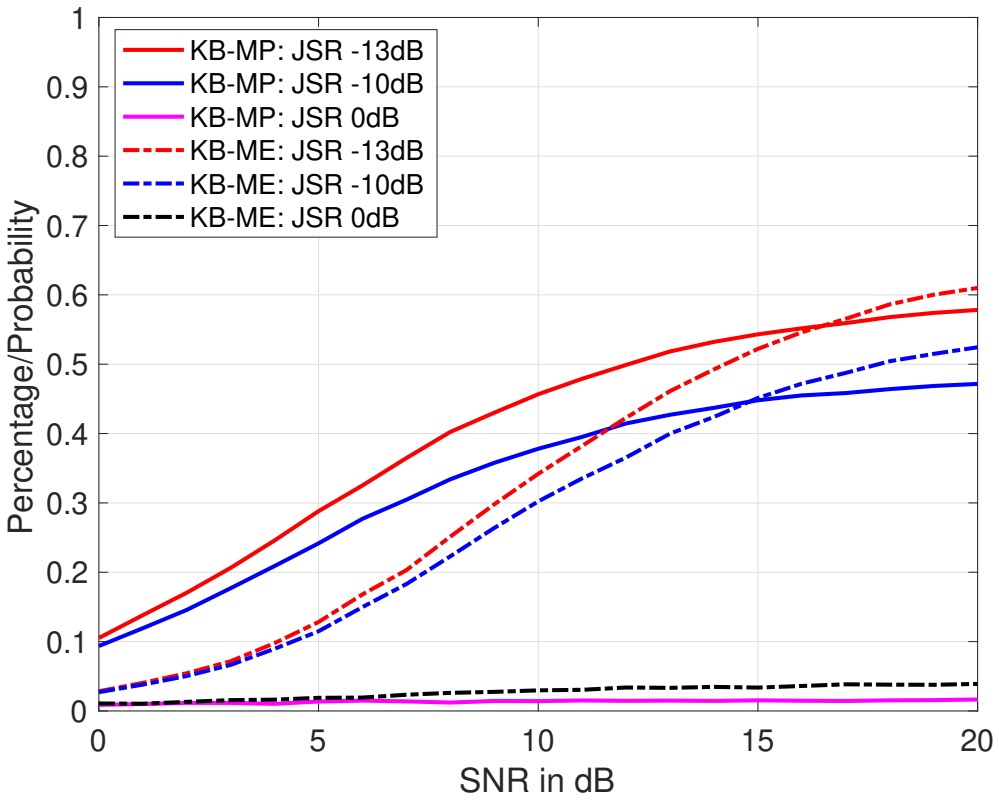

Figure 4.3. P_d results of Experiment 3, where $p_{mx} = 0.9$ and JSR is varied at -13 dB, -10 dB, and 0 dB.

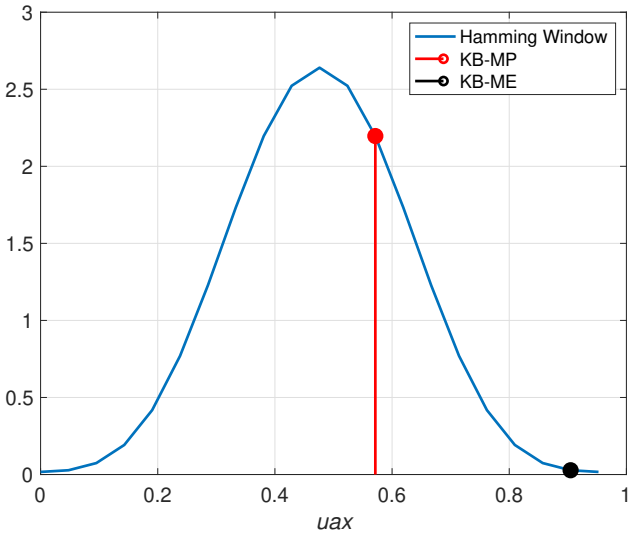

Figure 4.4. Interference power density model: Hamming window showing which angles u_k and u_{ke} are steered to.

4.2.2 Varying JNR

For the fourth experiment, p_{mx} = 0.9 and jammer-to-noise ratio (JNR) is varied at -10 dB, 0 dB, and 3 dB. Again, it is shown in Figure 4.5 that interference significantly affects detection performance of both KB-MP and KB-ME techniques. Increasing JNR significantly lowers the detection performance of both KB-MP and KB-ME techniques. The Hamming window utilized for interference is shown in Figure 4.6. In this experiment, both KB-MP and KB-ME are steered to equal amounts of interference. Interestingly, the opposite crossover detection performance is observed even though both angles chosen by the techniques have the same amount of interference.

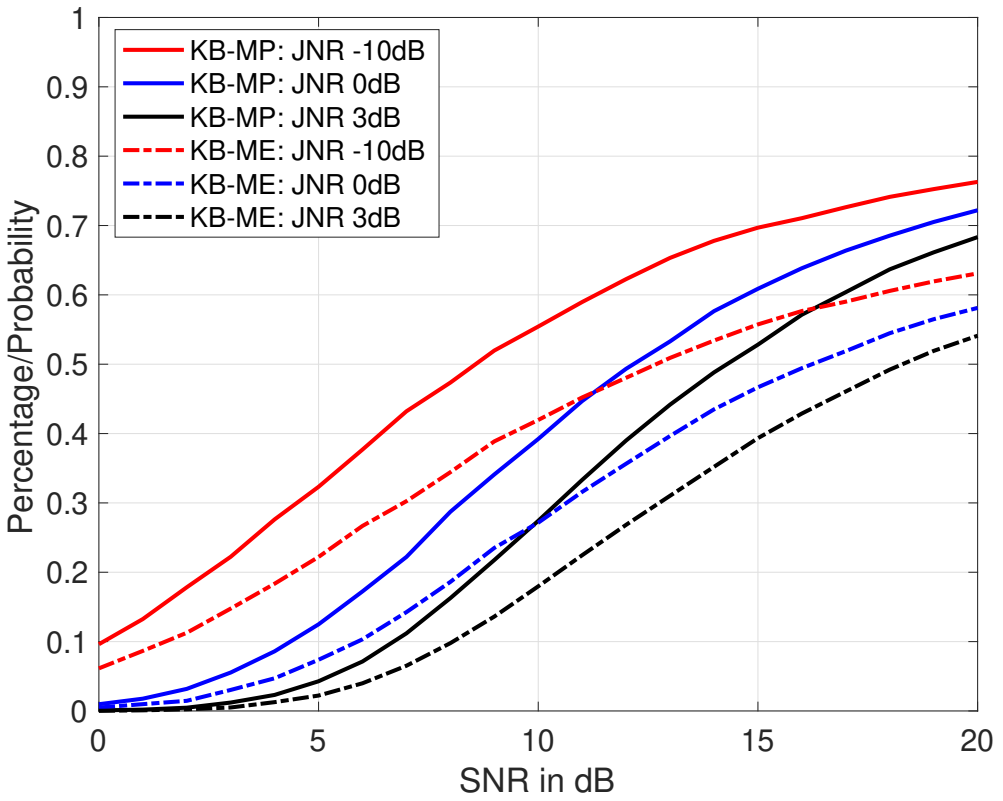

Figure 4.5. P_d results of Experiment 4, where $p_{mx} = 0.9$ and JNR is varied at -10 dB, 0 dB, and 3 dB.

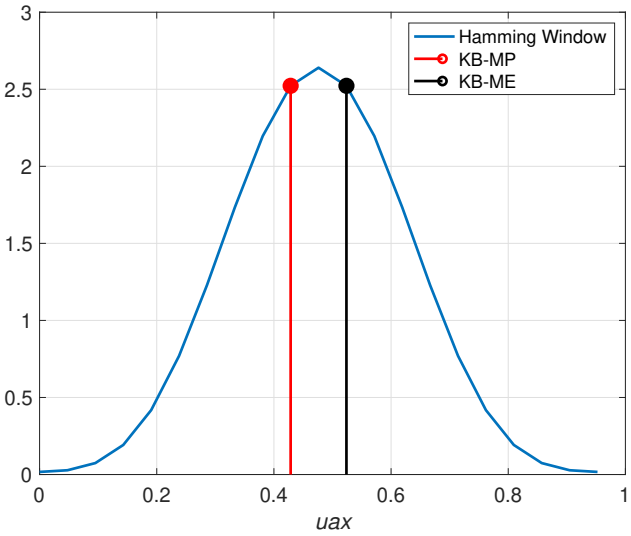

Figure 4.6. Interference power density model: Hamming window showing which angles u_k and u_{ke} are steered to.

CHAPTER 5:
Uniform Linear Array - Performance for Multiple Cells

5.1 Noise Only

Similarly to ULA single cell performance, we consider a signal comprised of the target return and thermal noise such that SNR is varied from 0 to 20 dB with 1 dB increments and desired $P_{fa} = 0.001$. Again, we utilize the model where there is maximum probability, p_{mx}, and corresponding maximum entropy. We compare the performance of KB-MP and KB-ME techniques while parameterizing p_{mx}, where $p_{mx} = 1$, 0.9, and 0.5. We conduct a Monte Carlo simulation, similar to Chapter 4, with 10,000 trials to quantify the probability of detection of a target present in the cell area as a function of SNR. In the Monte Carlo simulation, we introduce an indicator variable, p_i, as discussed in Chapter 4, that takes on the value of 1 (target present) and 0 (target not present). Due to multiple plane waves coming from multiple cells, we introduce an indicator variable to each steering vector. The steering vectors become:

$$\mathbf{vs_1} = p_1 \mathbf{vs_1} \tag{5.1}$$

$$\mathbf{vs_2} = p_2 \mathbf{vs_2} \tag{5.2}$$

$$\mathbf{vs_3} = p_3 \mathbf{vs_3}, \tag{5.3}$$

where $\mathbf{vs}_i$ are the steering vectors previously defined in Sections 2.3.2 and 2.4.2 and p_i is the indicator variable corresponding to the cell probability. The summed signal used to form the MVDR detector in the Monte Carlo simulation is given by

$$\mathbf{s_r} = \frac{1}{\sqrt{3}}(\mathbf{vs}_1 + \mathbf{vs}_2 + \mathbf{vs}_3). \tag{5.4}$$

Note that the scaling is such that the energy is normalized to one if all $p_i = 1$. Other weighting techniques are possible. The received signal in the simulation takes on the equation

$$\mathbf{x} = \mathbf{s}_r + \mathbf{n} \tag{5.5}$$

for KB-MP and

$$\mathbf{x} = \mathbf{s}_{re} + \mathbf{n} \tag{5.6}$$

for KB-ME.

The detection performance of a radar using KB-MP and a radar using KB-ME for the cell area chosen by each technique is shown in Figure 5.1. Like ULA single cell, KB-MP has higher probability of detection than KB-ME for multiple cells. When p_{mx} is 1, it is clear that KB-MP outperforms KB-ME but it isn't as clear that KB-MP will always outperform KB-ME when p_{mx} is 0.9. This is because the average probability may be considerably lower than 0.9. Recall that in our *a priori* model, the probabilities are randomly generated from 0 to p_{mx}. Thus when adjacent probabilities are added, the average probability can easily be lower than 0.9 such that entropy approach may actually choose a cell area where some cells have high probabilities although collectively, not necessarily, yield the maximum average. This is also the same reason why the detection probability does not approach 1 with the SNRs considered in the case of $p_{mx} = 1$. But an extension to higher SNR will converge to 1 for $p_{mx} = 1$. When p_{mx} is 0.5, both KB-MP and KB-ME have similar detection; thus, beamsteering may result in the same detection performance. Also, we see lower probability of detection performance when compared to results in Section 4.1 in the case of single cell using ULA. Again, this is due to having multiple cells where not all cells have high probabilities. For example, the chosen cell may have its center cell contain maximum probability and maximum entropy but one or more cells may contain lower probability or entropy since the average is used.

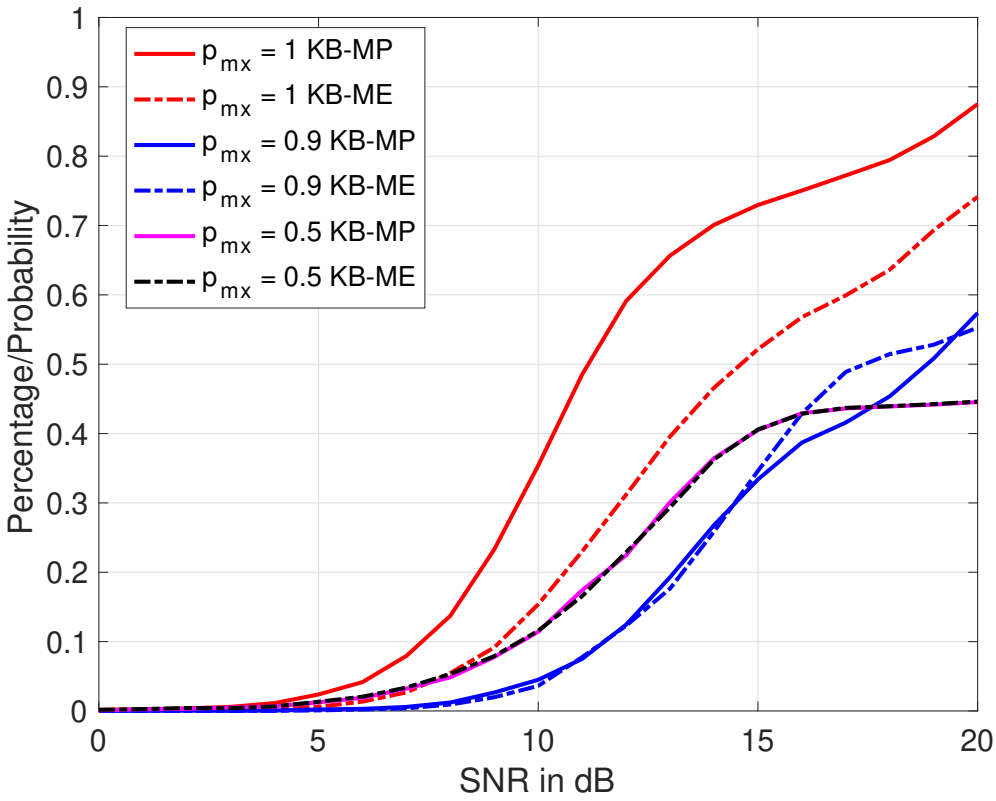

Figure 5.1. P_d results for Experiment 1: interference is thermal noise only, where p_{mx} represents the possible maximum target probability in the *a priori* model in the KB problem formulation.

5.2 Interference or Jamming

We consider a signal comprised of a steering vector, thermal noise, and interference. The received signal in the simulation takes on the equation

$$\mathbf{x} = p_{i,p}\mathbf{s}_r + \mathbf{n} + \mathbf{s}_{in} \tag{5.7}$$

for KB-MP and

$$\mathbf{x} = p_{i,e}\mathbf{s}_{re} + \mathbf{n} + \mathbf{s}_{in} \tag{5.8}$$

for KB-ME. With p_{mx} = 1, 0.9, and 0.5, we see in Figure 5.2 that allowing interference (jammers) to appear in all the angles including the cell area with the target returns significantly affects detection performance of both KB-MP and KB-ME. When p_{mx} = 0.5, both KB-MP and KB-ME have similar detection. For this particular simulation, we see in Figure 5.2 that detection performance for p_{mx} = 0.9 is slightly higher than for p_{mx} = 1. Recall that the probabilities are randomly generated. It is for this exact reason why averaging is used. For this particular experiment with p_{mx} values being close, it is easily possible that the maximum average chosen for p_{mx} = 0.9 is higher than p_{mx} = 1.

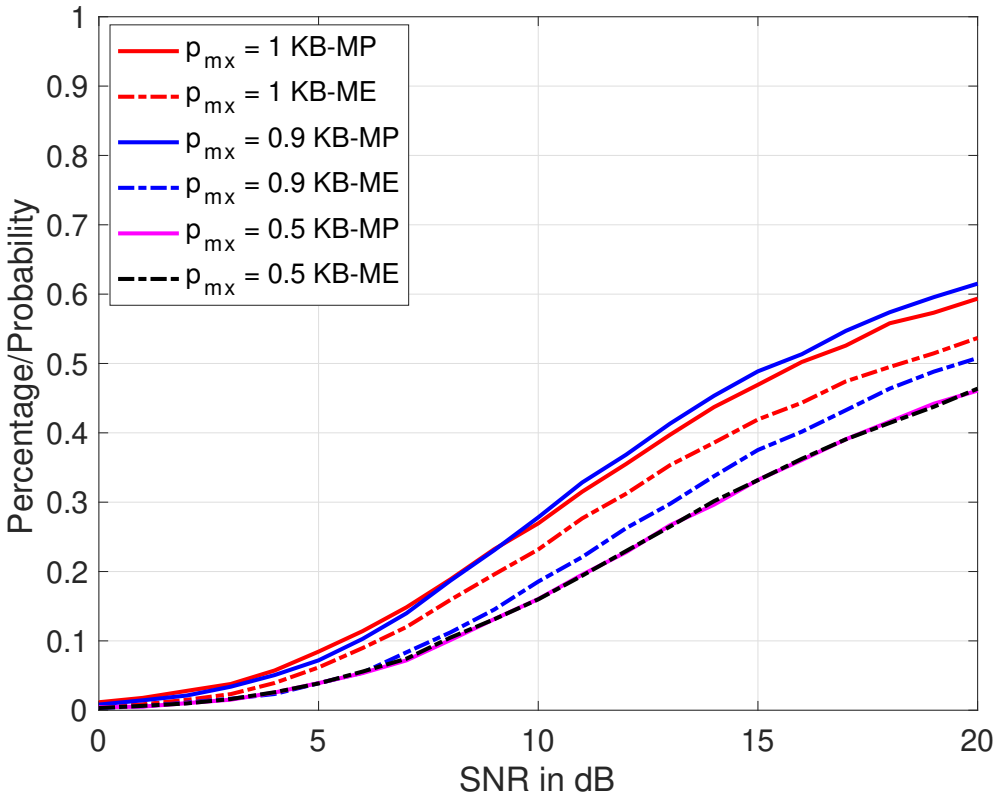

Figure 5.2. P_d results of Experiment 2: total interference consists of random jammer/interference and noise, where p_{mx} represents the possible maximum target probability in the *a priori* model in the KB problem formulation.

5.2.1 Varying JSR

As in Experiment 2, $p_{mx} = 0.9$ and JSR is varied at -13 dB, -10 dB, and 0 dB. Like in Section 4.2.1, it is shown in Figure 5.3 that interference significantly affects detection performance of both KB-MP and KB-ME. Increasing the jammer power significantly lowers the detection performance. The Hamming window utilized for interference is shown in Figure 5.4, where it is clear the cell chosen by KB-ME technique contains more interference than the cell chosen by KB-MP technique. Due to this and the interesting nature of the case of multiple cells to a beamwidth, we see in Figure 5.3 that as SNR and JSR are increased, a crossover in performance occurs. At a very large SNR, P_d for KB-MP is better than KB-ME. This is due to the fact that the angles chosen by KB-ME have more interference as shown in Figure 5.4. For JSR = 0 dB, P_d for KB-MP and KB-ME are close to zero. The difference between the jammer power and signal power is substantial that detection performance is poor.

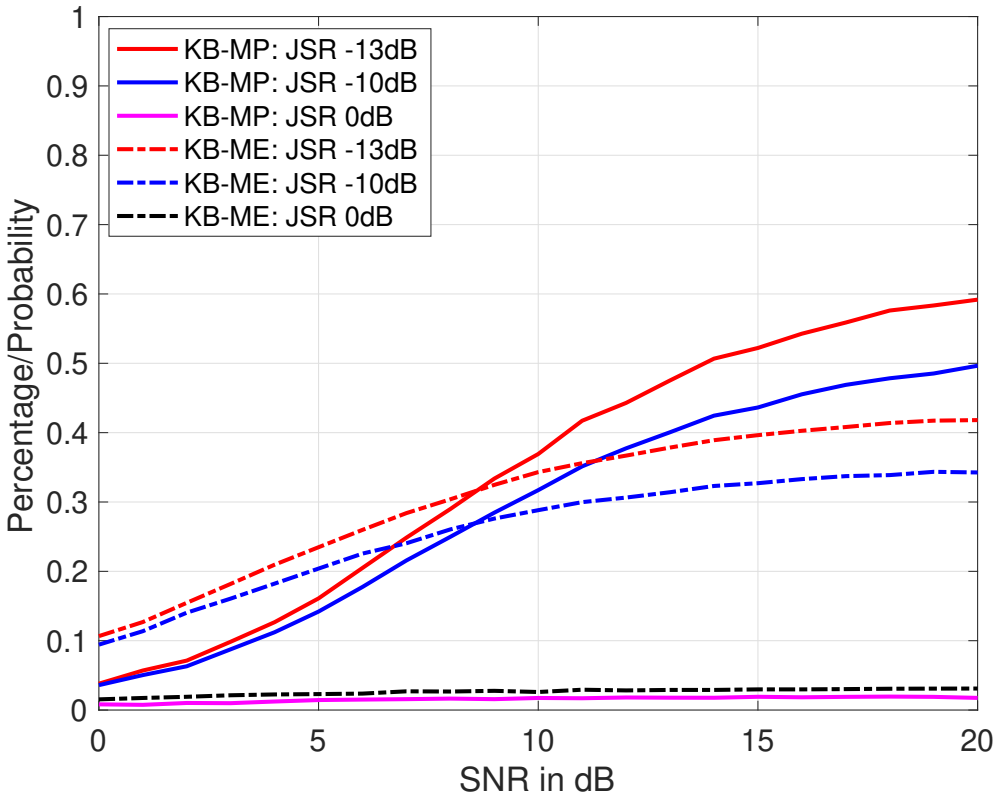

Figure 5.3. P_d results of Experiment 3, where $p_{mx} = 0.9$ and JSR is varied at -13 dB, -10 dB, and 0 dB.

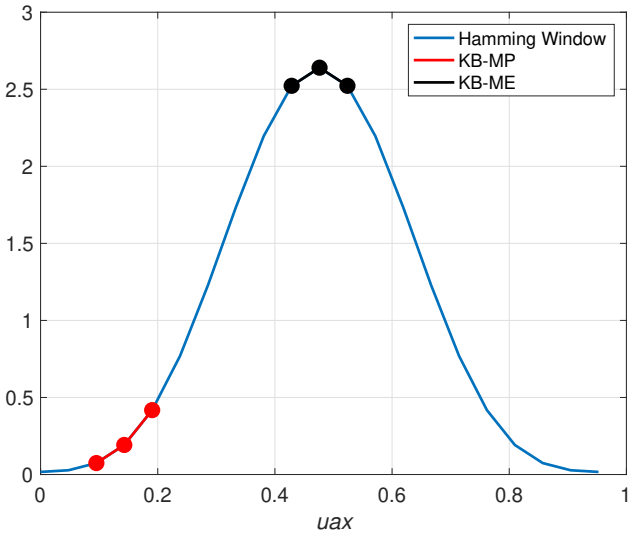

Figure 5.4. Interference power density model: Hamming window showing which angles u_k and u_{ke} are steered to.

5.2.2 Varying JNR

In the fourth experiment, p_{mx} = 0.9 and JNR is varied at -10 dB, 0 dB, and 3 dB. Again, it is shown in Figure 5.5 that interference significantly affects detection performance of both KB-MP and KB-ME where increasing JNR significantly lowers the detection performance of both KB-MP and KB-ME. The Hamming window utilized for interference is shown in Figure 5.6, where it is clear the cell chosen by KB-MP technique contains more interference than the cell chosen by KB-ME technique. In Figure 5.5, we see that KB-MP has better detection performance than KB-ME despite the location of the cell area in regards to interference. This can happen when the cell area probability distribution for one approach, in this case KB-MP, is vastly different than the other approach, KB-ME. In other words, P_d is greatly affected by both *a priori* cell probabilities and interference power. As mentioned before, ultimately, the performance of KB-MP and KB-ME depends on the value of both parameters.

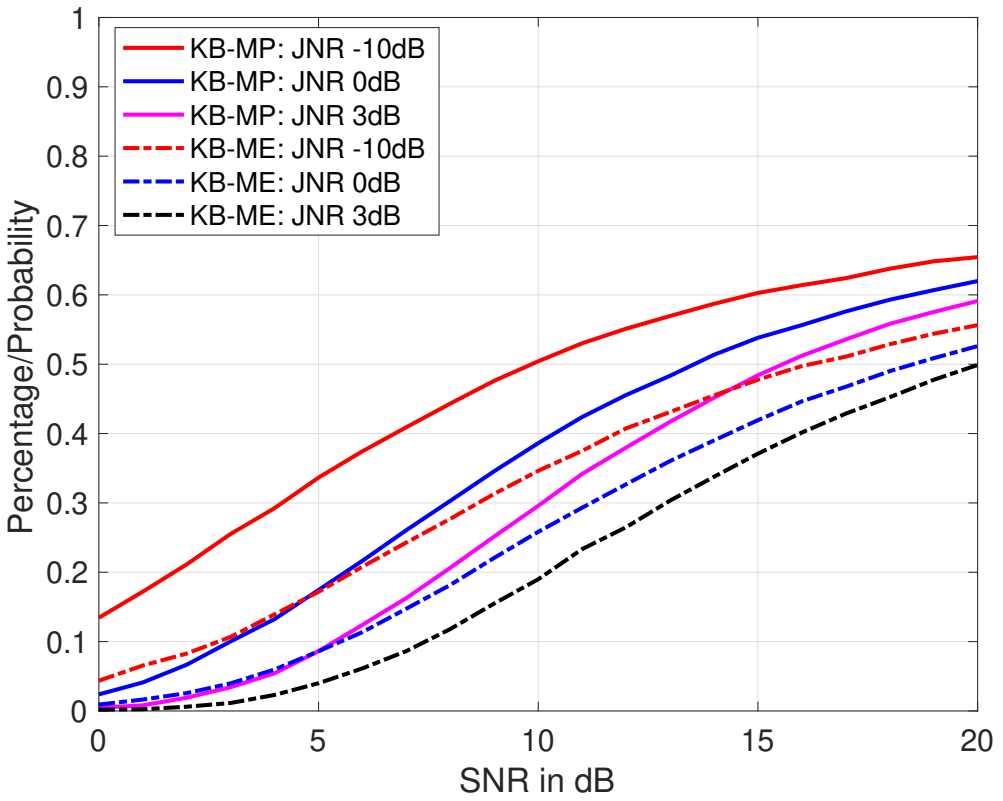

Figure 5.5. P_d results of Experiment 4, where $p_{mx} = 0.9$ and JNR is varied at -10 dB, 0 dB, and 3 dB.

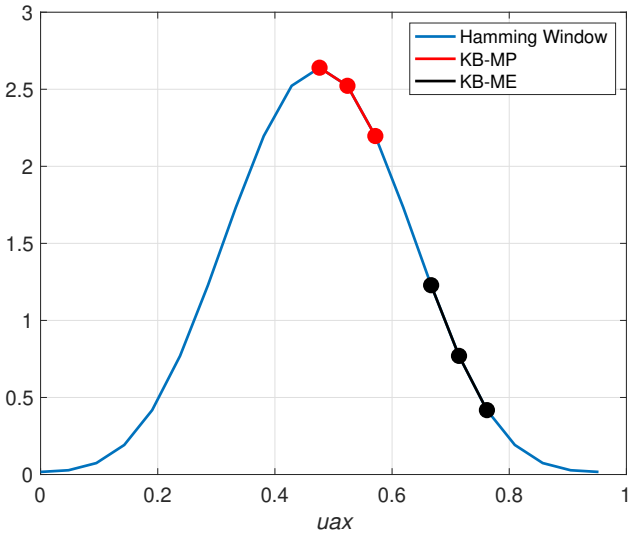

Figure 5.6. Interference power density model: Hamming window showing which angles u_k and u_{ke} are steered to.

CHAPTER 6:
Uniform Planar Array - Single Cell Performance

6.1 Noise Only

We consider a signal comprised of the target return and thermal noise such that SNR is varied from 0 to 20 dB with 1 dB increments and desired $P_{fa} = 0.001$. In terms of scenario-specific probability models that describe the search area, we assume a model with randomly generated cell probabilities for the maximum probability, p_{mx}, with corresponding maximum entropy. We then compare the performance of KB-MP and KB-ME while parameterizing p_{mx}, where p_{mx} = 1, 0.9, and 0.5. Again, since the values in the probability map are randomly generated, p_{mx} is not the guaranteed maximum realization in the simulation. We introduce a probability scenario variable, p_s, that takes on the maximum realization value in the simulation. We conduct a Monte Carlo simulation with 10,000 trials to quantify the probability of detection of a target present in that cell as a function of SNR. There is a subtle yet significant difference from a simple detection problem that we consider in this work. Recall that while *a priori* knowledge informs us of cell probability, it does not guarantee the presence of a target unlike the conditional target present hypothesis in the common detection problem. Thus, in the Monte Carlo simulation, we introduce an indicator variable, p_i, that takes on the value of 1 (target present) and 0 (target not present). For example, if p_s is used, then the ratio of 1's to the number of Monte Carlo trials converges to p_s as the number of trials get large. Then, the received signal in the simulation takes on the equation

$$\mathbf{x} = p_{i,p}\mathbf{s}_r + \mathbf{n} \tag{6.1}$$

for KB-MP and

$$\mathbf{x} = p_{i,e}\mathbf{s}_{re} + \mathbf{n} \tag{6.2}$$

for KB-ME, where $p_{i,p}$ and $p_{i,e}$ are the indicator variables corresponding to the two techniques. The comparison of the probability of detection of a radar using KB-MP and a radar using KB-ME for the cell chosen by each technique is shown in Figure 6.1. It is clear that KB-MP has higher probability of detection than KB-ME for p_{mx} of 1 and 0.9. When p_{mx} is

0.5, both KB-MP and KB-ME have similar detection thus beamsteering to either cell would result in the same detection performance.

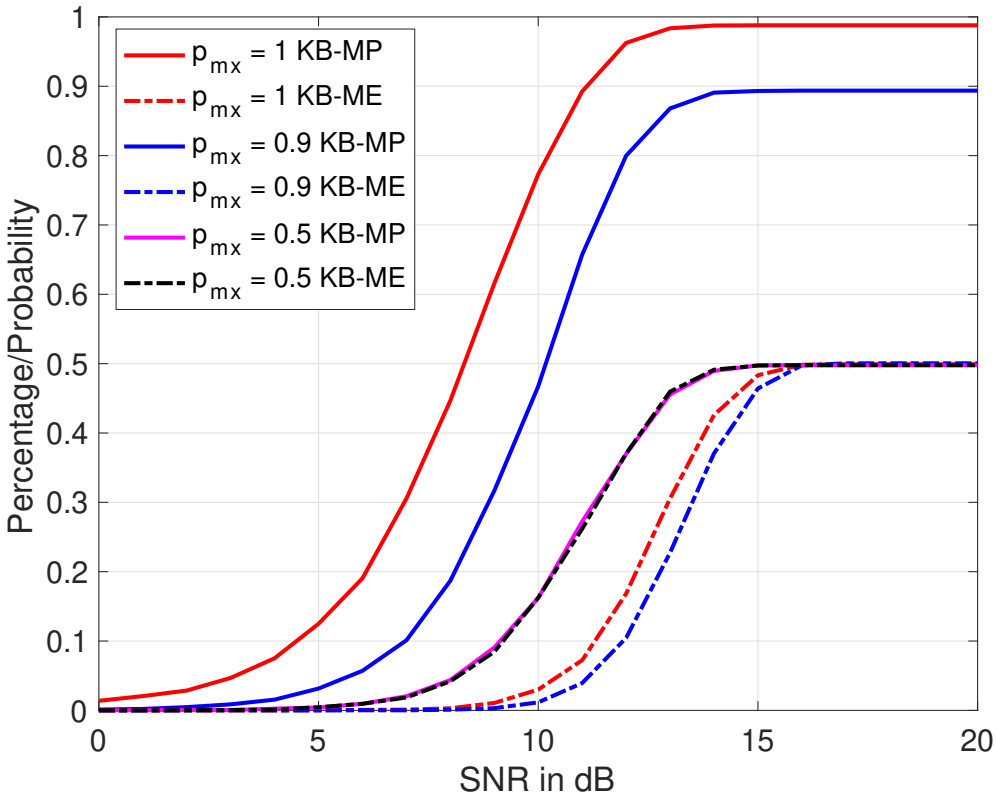

Figure 6.1. P_d results for Experiment 1: interference is thermal noise only, where p_{mx} represents the possible maximum target probability in the *a priori* model in the KB problem formulation.

6.2 Interference or Jamming

Next we consider a signal comprised of a steering vector, thermal noise, and interference. The received signal in the simulation takes on the equation

$$\mathbf{x} = p_{i,p}\mathbf{s}_r + \mathbf{n} + \mathbf{s}_{in} \tag{6.3}$$

for KB-MP and

$$\mathbf{x} = p_{i,e}\mathbf{s}_{re} + \mathbf{n} + \mathbf{s}_{in} \tag{6.4}$$

for KB-ME. With p_{mx} = 1, 0.9, and 0.5, we see in Figure 6.2 that allowing interference (jammers) to appear in all the angles including the angle with the target return significantly affects detection performance of both KB-MP and KB-ME. When p_{mx} = 0.5, both KB-MP and KB-ME have similar detection.

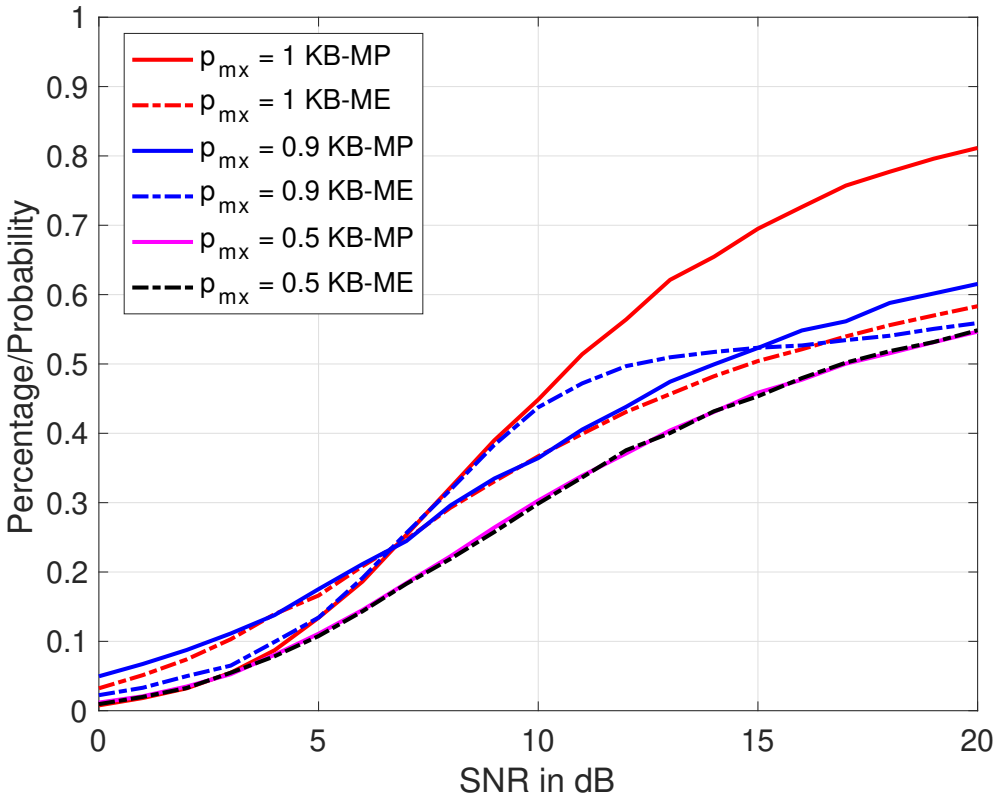

Figure 6.2. P_d results of Experiment 2: total interference consists of random jammer/interference and noise, where p_{mx} represents the possible maximum target probability in the *a priori* model in the KB problem formulation.

6.2.1 Varying JSR

As in Experiment 2, p_{mx} = 0.9 and JSR is varied at -13 dB, -10 dB, and 0 dB. We see in Figure 6.3, that interference significantly affects detection performance of both KB-MP

and KB-ME, but is more apparent in the KB-ME technique. Increasing the jammer power compared to the signal power significantly lowers the detection performance. The 2-D Hamming window utilized for interference is shown in Figure 6.4, where the cell chosen by KB-MP technique contains equal amounts of interference as the cell chosen by KB-ME technique. Due to this, we see in Figure 6.3 that regardless of increasing SNR and/or JSR, KB-MP has better detection performance. This situation means that KB-MP is more likely to have a higher cell probability than KB-ME.

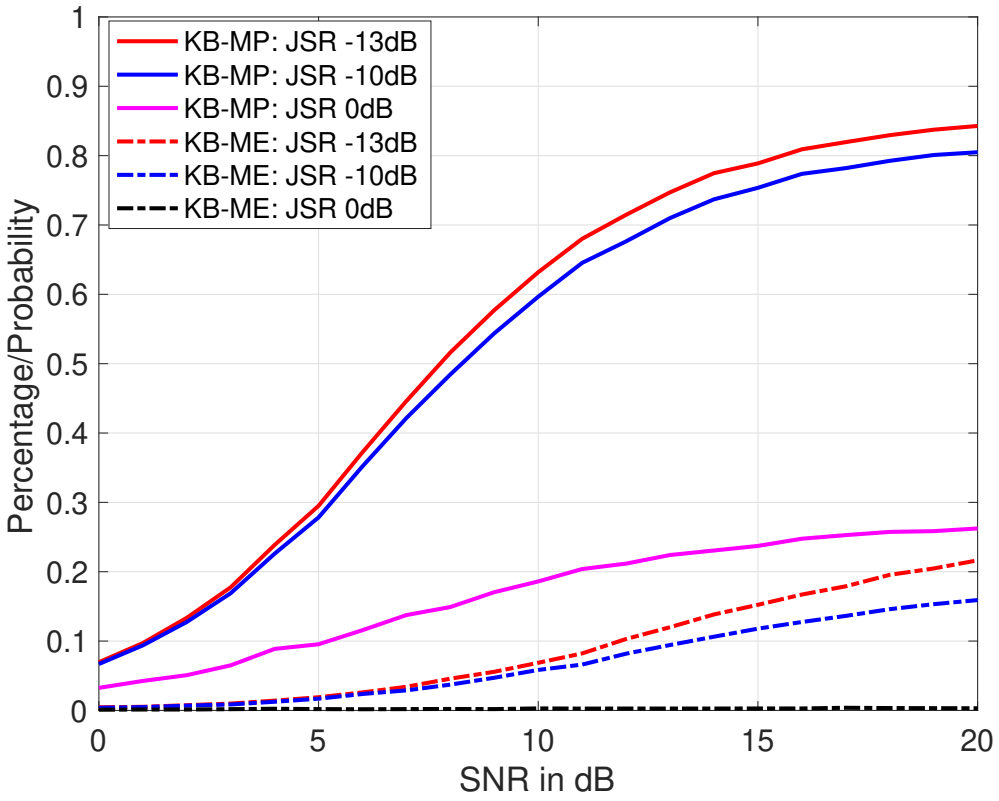

Figure 6.3. P_d results of Experiment 3, where $p_{mx} = 0.9$ and JSR is varied at -13 dB, -10 dB, and 0 dB.

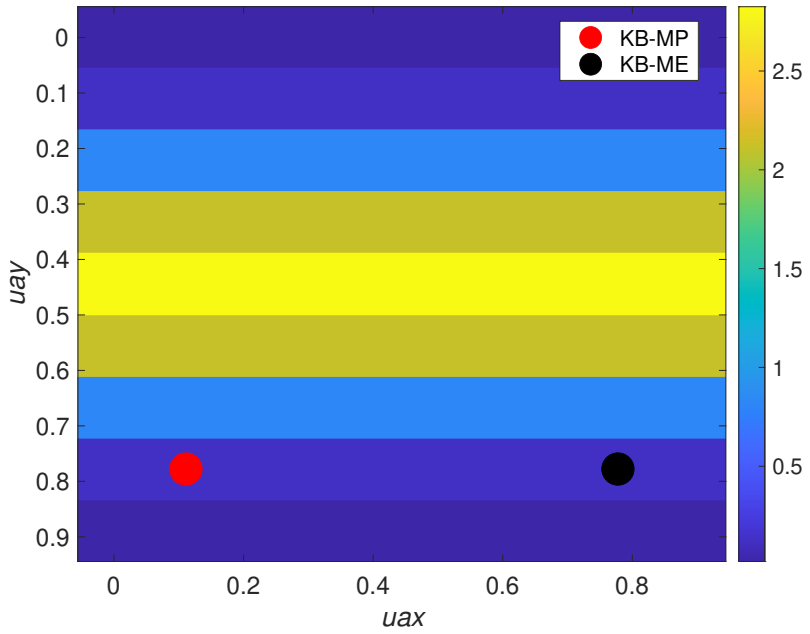

Figure 6.4. Interference power density model: 2-D Hamming window showing which angles u_k and u_{ke} are steered to.

6.2.2 Varying JNR

For the fourth experiment, p_{mx} = 0.9 and JNR is varied at -10 dB, 0 dB, and 3 dB. Again, it is shown in Figure 6.5 that interference significantly affects detection performance of both KB-MP and KB-ME techniques. Increasing the power of JNR significantly lowers the detection performance of both KB-MP and KB-ME techniques. The 2-D Hamming window utilized for interference is shown in Figure 6.6, where it is clear the cell chosen by KB-MP technique contains more interference than the cell chosen by KB-ME technique. Despite having more interference, KB-MP has better detection performance than KB-ME. Thus, P_d is affected by both *a priori* knowledge and interference; but sometimes, one factor dominates the other as to which factor significantly affects detection performance. In this case, *a priori* knowledge is the dominating factor in the analysis of this performance experiment.

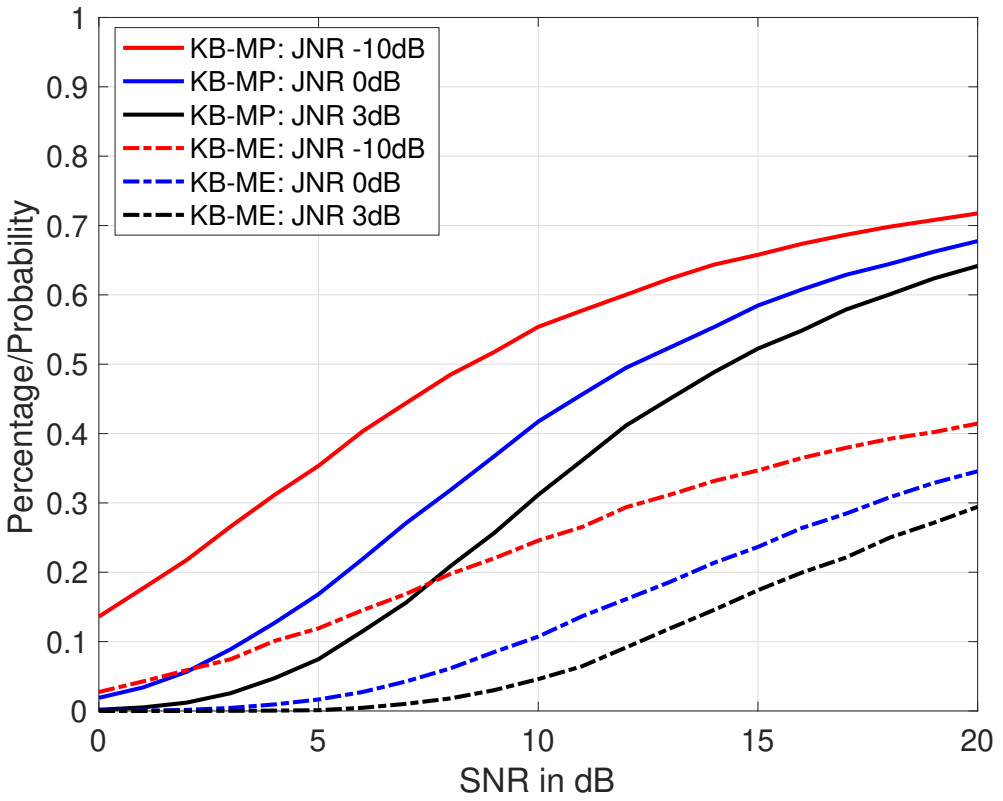

Figure 6.5. P_d results of Experiment 4, where $p_{mx} = 0.9$ and JNR is varied at -10 dB, 0 dB, and 3 dB.

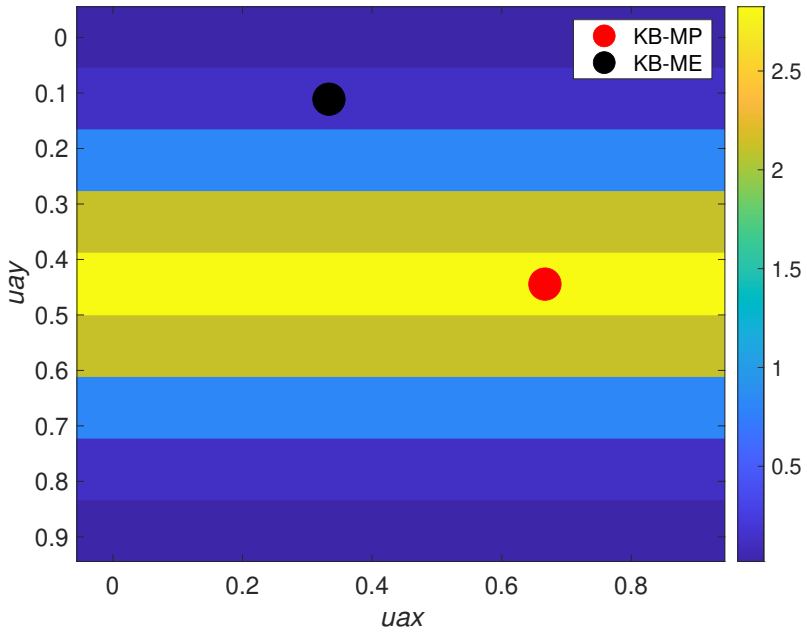

Figure 6.6. Interference power density model: 2-D Hamming window showing which angles u_k and u_{ke} are steered to.

THIS PAGE INTENTIONALLY LEFT BLANK

CHAPTER 7:
Uniform Planar Array - Performance for Multiple Cells

As in Chapter 5, the return signal corresponds to a cell area, where we introduce an indicator variable, p_i, that takes on the value of 1 (target present) and 0 (target not present) to each component of the signal. The steering vectors become

$$\mathbf{vs} = p_{i,p}\mathbf{vs}_i \tag{7.1}$$

for KB-MP and

$$\mathbf{vse} = p_{i,e}\mathbf{vse_i} \tag{7.2}$$

for KB-ME, where $\mathbf{vs}_i$ and $\mathbf{vse}_i$ are the steering vectors previously defined in Sections 2.3.4 and 2.4.4 and $p_{i,p}$ and $p_{i,e}$ are the indicator variables corresponding to the two techniques. The summed signal used to form the MVDR detector in the Monte Carlo simulation is given as

$$\mathbf{s_r} = \frac{1}{\sqrt{4}}(\mathbf{vs}_1 + \mathbf{vs}_2 + \mathbf{vs}_3 + \mathbf{vs}_4) \tag{7.3}$$

for KB-MP and

$$\mathbf{s_{re}} = \frac{1}{\sqrt{4}}(\mathbf{vse}_1 + \mathbf{vse}_2 + \mathbf{vse}_3 + \mathbf{vse}_4) \tag{7.4}$$

for KB-ME.

7.1 Noise Only

For noise only, we consider a signal comprised of the target return and thermal noise such that SNR is varied from 0 to 20 dB with 1 dB increments and desired P_{fa} = 0.001. We utilize the model where there is maximum probability, p_{mx}, which of course has a corresponding maximum entropy. We then compare the performance of KB-MP and KB-ME techniques while parameterizing p_{mx}, where p_{mx} = 1, 0.9, and 0.5. Since the values in the probability map are randomly generated, p_{mx} is not the guaranteed maximum realization in the simulation. We conduct a Monte Carlo simulation with 10,000 trials to quantify the probability of detection of a target present in that cell as a function of SNR. While *a priori* knowledge informs us of cell probability, it does not guarantee the presence of a target.

Then, the received signal in the simulation takes on the equation

$$\mathbf{x} = \mathbf{s}_r + \mathbf{n} \tag{7.5}$$

for KB-MP and

$$\mathbf{x} = \mathbf{s}_{re} + \mathbf{n} \tag{7.6}$$

for KB-ME.

The detection performance of a radar using KB-MP and a radar using KB-ME for the cells chosen by each technique is shown in Figure 7.1. Like previous performance results, KB-MP has higher probability of detection than KB-ME for multiple cells. When p_{mx} = 1 and 0.9, it is clear that KB-MP outperforms KB-ME. When p_{mx} is 0.5, both KB-MP and KB-ME have similar detection; thus, beamsteering to either cells would result in the same detection performance. From Figure 7.1, we see probability of detection performance is reduced at high powers of SNR, this is due to having multiple cells where not all cells have high probabilities. For example, the chosen cell area may have its center cell contain maximum probability and maximum entropy but one or more cells may contain lower probability or entropy since the average is used.

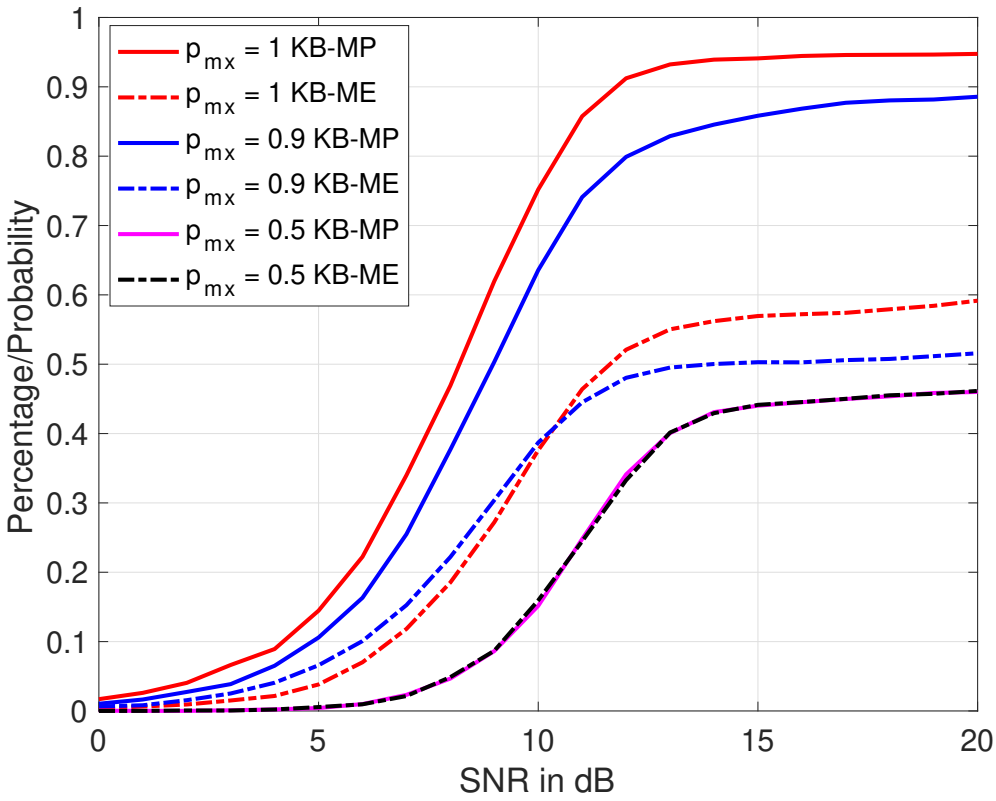

Figure 7.1. P_d results for Experiment 1: interference is thermal noise only, where p_{mx} represents the possible maximum target probability in the *a priori* model in the KB problem formulation.

7.2 Interference or Jamming

We consider a signal comprised of a steering vector, thermal noise, and interference. The received signal in the simulation takes on the equation

$$\mathbf{x} = p_{i,p}\mathbf{s}_r + \mathbf{n} + \mathbf{s}_{in} \tag{7.7}$$

for KB-MP and

$$\mathbf{x} = p_{i,e}\mathbf{s}_{re} + \mathbf{n} + \mathbf{s}_{in} \tag{7.8}$$

for KB-ME. With p_{mx} = 1, 0.9, and 0.5, we see in Figure 7.2, that allowing interference (jammers) to appear in all the angles including the cell area with the target returns significantly affects detection performance of both KB-MP and KB-ME. When p_{mx} = 0.5, both KB-MP and KB-ME have similar detection. When p_{mx} = 1 and 0.9, we see a crossover in performance of maximum probability for both KB-MP and KB-ME as SNR increases. Overall, KB-MP has better detection than KB-ME.

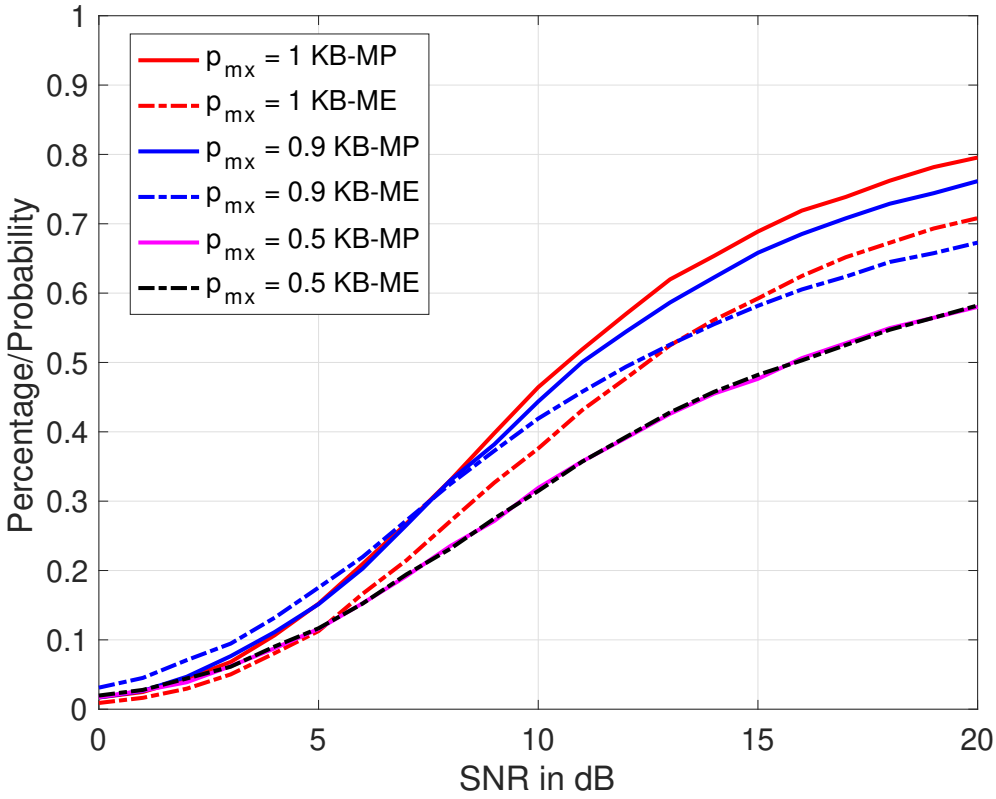

Figure 7.2. P_d results of Experiment 2: total interference consists of random jammer/interference and noise, where p_{mx} represents the possible maximum target probability in the *a priori* model in the KB problem formulation.

7.2.1 Varying JSR

As in Experiment 2, p_{mx} = 0.9 and JSR is varied at -13 dB, -10 dB, and 0 dB. Like in previous sections, it is shown in Figure 7.3 that interference significantly affects detection

performance of both KB-MP and KB-ME. Increasing the jammer power signal significantly lowers the detection performance. The 2-D Hamming window utilized for interference is shown in Figure 7.4, where it is clear the cell chosen by KB-MP technique contains more interference than the cell chosen by KB-ME technique. As in Section 4.2.1, we have a very similar P_d. As SNR and JSR are increased, we have a crossover in performance as illustrated in Figure 7.3. Typically, as observed already, KB-MP has better detection than KB-ME. Note however, that at very large SNR, P_d for KB-ME is better than KB-MP. This is because the angles chosen by KB-ME have less interference as shown in Figure 7.4. In other words, P_d is affected by both *a priori* cell probabilities and interference power. As mentioned before, ultimately, the performance of KB-MP and KB-ME depends on the value of both parameters.

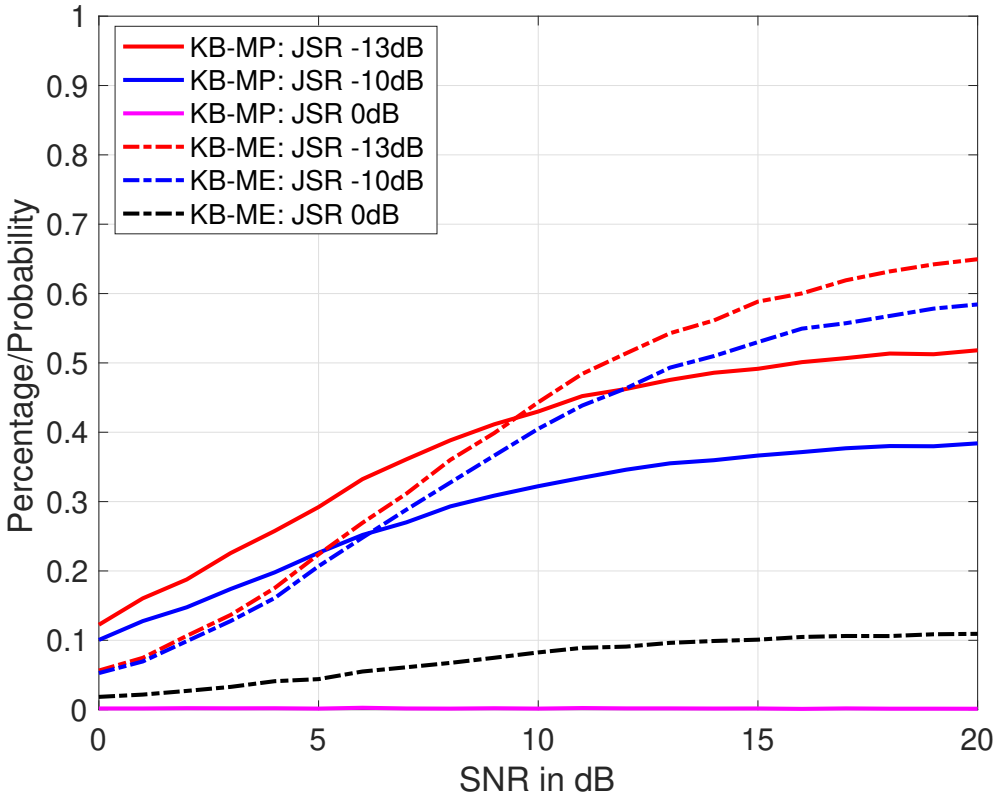

Figure 7.3. P_d results of Experiment 3, where $p_{mx} = 0.9$ and JSR is varied at -13 dB, -10 dB, and 0 dB.

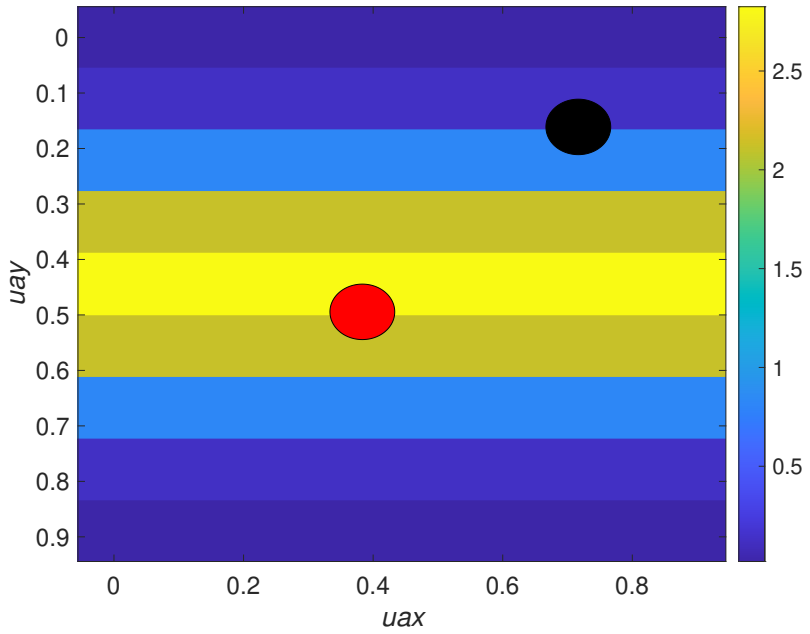

Figure 7.4. Interference power density model: 2-D Hamming window showing which angles u_k and u_{ke} are steered to.

7.2.2 Varying JNR

In the fourth experiment, p_{mx} = 0.9 and JNR is varied at -10 dB, 0 dB, and 3 dB. We see in Figure 7.5 that interference significantly affects detection performance of both KB-MP and KB-ME techniques. Increasing the power of JNR significantly lowers the detection performance of both KB-MP and KB-ME. The 2-D Hamming window utilized for interference is shown in Figure 7.6, where the cell chosen by KB-MP technique contains equal amounts of interference as the cell chosen by KB-ME technique. Typically, as seen in previous results, when both KB-MP and KB-ME have equal parameters, meaning *a priori* cell probabilities and interference power, KB-MP outperforms KB-ME in detection results. In Figure 7.5, KB-MP, does in fact, have better detection performance than KB-ME.

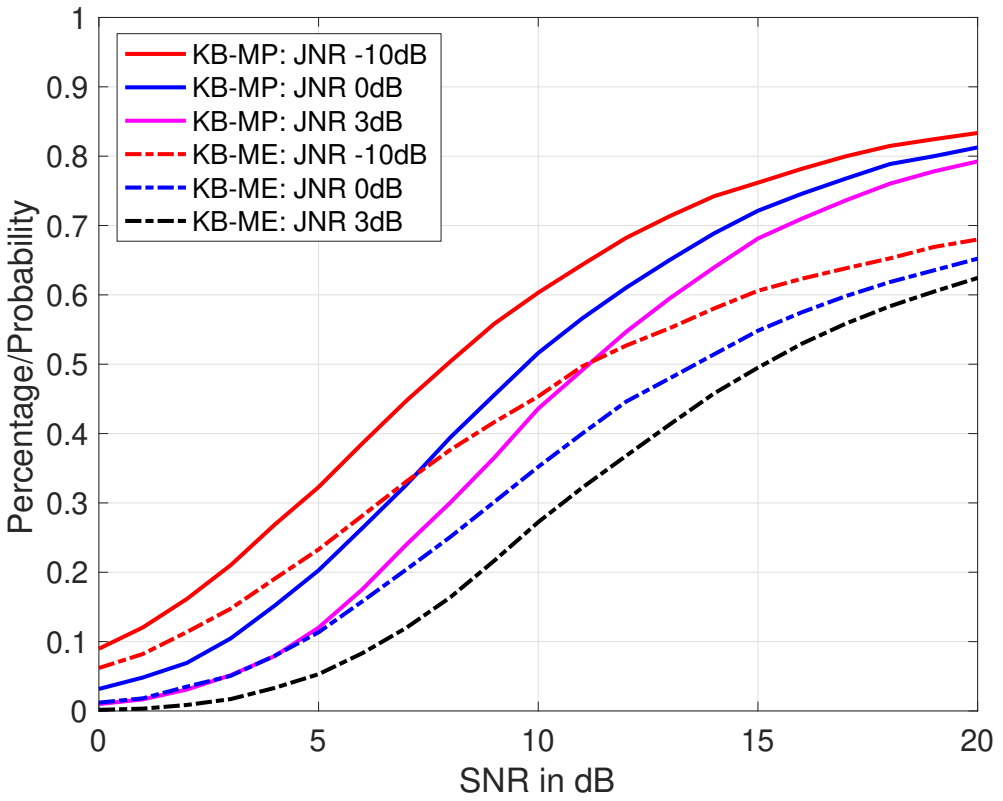

Figure 7.5. P_d results of Experiment 4, where $p_{mx} = 0.9$ and JNR is varied at -10 dB, 0 dB, and 3 dB.

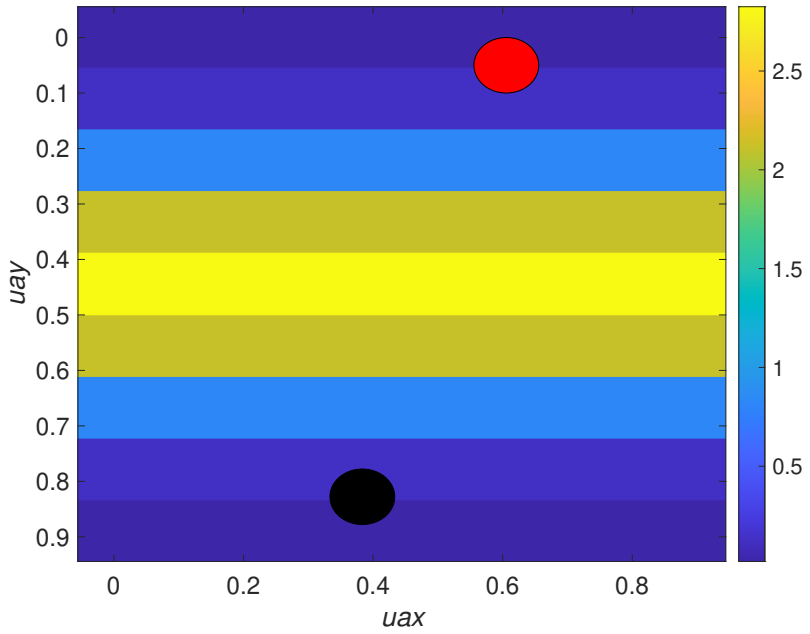

Figure 7.6. Interference power density model: 2-D Hamming window showing which angles u_k and u_{ke} are steered to.

CHAPTER 8:
Summary

In this thesis, we introduced two different approaches for KB adaptive beamsteering to enhance detection and mitigate interference. While prior research used the uncertainty-based decision functions for search and track to evaluate performance, we introduced a selection algorithm based directly on cell prior probability for search and detection which we called KB-MP (while KB-ME stands for maximum entropy). We extended the 1-D ULA to a 2-D UPA, where we investigated detection based on a single cell versus a cell area containing multiple cells.

We saw very similar detection performance results for both the ULA and the UPA. Generally, KB-MP performed better than KB-ME in terms of detection where the probability map had cells with $p_{mx} > 0.5$. When $p_{mx} = 0.5$, we noticed KB-MP and KB-ME have similar detection results. For scenarios where jammers/interference were allowed in the same angular area as the signal, detection performance was reduced.

We demonstrated in this thesis that adaptive beamsteering, when allowed to capitalize on the probability map, can improve detection probability significantly and mitigate random interference and jammer models for both 1-D and 2-D radar systems. Overall, P_d is affected by both *a priori* cell probabilities and the power of interference; and the performance of KB-MP and KB-ME depend on the value of both parameters.

The techniques presented in this thesis have many opportunities for future work. One recommendation for future work is to extend this model to a 3-D cognitive radar system where it can be used for not only search and detection, but also search and track. Another option for future work is to incorporate this model into a non-uniform array. This model can be used with other previous thesis works on classification and angle of arrival problems.

THIS PAGE INTENTIONALLY LEFT BLANK

List of References

[1] S. Haykin, "Cognitive radar: A way of the future," *IEEE Signal Processing Magazine*, vol. 23, no. 1, pp. 30–40, January 2006.

[2] G. T. Capraro, A. Farina, H. Grifiths, and M. C. Wicks, "Knowledge-based radar signal and data processing: A tutorial review," *IEEE Signal Processing Magazine*, vol. 23, no. 1, pp. 18–29, January 2006.

[3] A. Charlish, H. Grifiths, and N. A. Goodman, "Cognitive radar (radar cognitif)," Science and Technology Orgazination North Atlantic Treaty Organization, Neuilly-sur-Seine Cedex, France, STO-TR-SET 227, October 2020.

[4] K. L. Bell, C. J. Baker, G. E. Smith, J. T. Johnson, and M. Rangaswamy, "Cognitive radar framework for target detection and tracking," *IEEE Journal of Selected Topics in Signal Processing*, vol. 9, no. 8, pp. 1427–1439, Dec. 2015.

[5] R. A. Romero and N. A. Goodman, "Cognitive radar network: Cooperative adaptive beamsteering for integrated search-and-track application," *IEEE Transactions on Aerospace and Electronic Systems*, vol. 49, no. 2, pp. 915–931, April 2013.

[6] Z. W. Johnson and R. A. Romero, "Uncertainty function design for adaptive beamsteering cognitive radar," *2020 IEEE International Radar Conference (RADAR)*, pp. 1058–1062, April 2020.

[7] H. L. Van Trees, *Optimum Array Processing. Part IV of Detection, Estimation, and Modulation Theory*. New York, USA: John Wiley and Sons, Inc., 2002.

[8] G. Y. Hermann, "Various approaches to measurement uncertainty: A comparison," *IEEE 9th International Symposium on Intelligent Systems and Informatics*, pp. 377–380, September 2011.

[9] C. H. Bennett and P. W. Shor, "Quantum information theory," *IEEE Transactions on Information Theory*, vol. 44, no. 6, pp. 2724–2742, October 1998.

THIS PAGE INTENTIONALLY LEFT BLANK

Initial Distribution List

1. Defense Technical Information Center
   Ft. Belvoir, Virginia

2. Dudley Knox Library
   Naval Postgraduate School
   Monterey, California